INTERNATIONAL JOURNAL FOR NUMERICAL METHODS IN ENGINEERING
Int. J. Numer. Meth. Engng (2014)
Published online in Wiley Online Library (wileyonlinelibrary.com). DOI: 10.1002/nme.4803

An extended Layerwise method for composite laminated beams with multiple delaminations and matrix cracks

D. H. Li, Y. Liu and X. Zhang*

School of Aerospace Engineering, Tsinghua University, Beijing 100084, China

SUMMARY

For the delamination and matrix crack prediction of composite laminated structures, the methods based on the damage mechanics and fracture mechanics are most commonly used. However, there are very few methods that can accurately simulate the delaminations together with matrix cracks, although the in-plane matrix cracks always exist alongside the delaminations under impact loading. In this work, an extended layerwise method is developed to model the composite laminated beam with multiple delaminations and matrix cracks. In the displacement field, the nodes in the thickness direction are located at the middle surface of each single layer, the top surface and the bottom surface of the composite beams. The displacement field contains the linear Lagrange interpolation functions, the one-dimensional weak discontinuous function and strong discontinuous function. The strong and weak discontinuous function are applied to model the displacement discontinuity induced by delaminations and the strain discontinuity induced by the interface between the layers, respectively. Because the nodes in the thickness direction are located at the middle surface of each single layer, the extended layerwise method can be conveniently employed to deal with the in-plane matrix cracks combined with the extend FEM. Copyright © 2014 John Wiley & Sons, Ltd.

Received 15 May 2014; Revised 15 July 2014; Accepted 8 September 2014

KEY WORDS: composite beam; delaminations; matrix cracks; Layerwise theory

1. INTRODUCTION

The behavior of composite laminated structures under low velocity impact is of concern in recent years, because the internal damages induced by low velocity impact such as a dropped tool or debris from runways could reduce the strength of the structure significantly and furthermore these internal damages are not visibly detectable. If the impact-induced internal damages are not detected and repaired in time, the damage area will continuously grow and finally lead to complete structural collapse. A number of investigations have demonstrated that upon impact by a low velocity [1–11], the main part of damage in the composite laminates is caused by the matrix cracks and delaminations, because the tensile failure strength of the fiber is high, and the damage induced by fiber breakage is generally very limited and confined to the region under and near the contact area between the impactor and the composite laminates. Choi *et al.* [7] reported that the intraply matrix cracking is the initial damage mode. Because the matrix cracks induce local stress concentrations at crack tips, the delaminations initiates once the matrix cracks reach the interface between the ply groups having different fiber orientations. Joshi and Sun [12] presented a typical matrix cracks and delaminations pattern resulted from low impact, as shown in Figure 1.

To model the matrix cracks and delaminations within the laminate structures, two methods based on the damage mechanics and the fracture mechanics were usually used [13–21]. In the damage mechanics methods, the stresses regimes at the layer interfaces are used to predict the onset of

*Correspondence to: X. Zhang, School of Aerospace Engineering, Tsinghua University, Beijing 100084, China.
†E-mail: xzhang@tsinghua.edu.cn

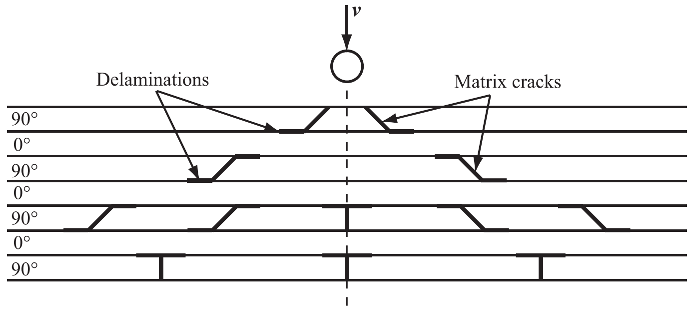

Figure 1. Typical matrix cracks and delaminations pattern resulted from low impact [12].

delamination by macro-scopic damage initiation criteria, such as Choi-Wu [6, 7] and Hashin criteria [22, 23]. The cumulative effect of delamination can be described by the material degradation models at failure material point. The implementation of the damage mechanics methods is very simple. Because the damage is incorporated within the constitutive model, the damage mechanics methods are easily adapted to numerical approaches such as the FEM. But the real extension process of delamination can not be observed in the damage mechanics methods. In the fracture mechanics methods, linear elastic fracture mechanics (LEFM) is commonly applied for the problem of delamination. Although the fracture mechanics predictions for metallic materials has been widely adopted because of its relative simplicity and accuracy, it is not true for the delamination problem of composite laminates. LEFM is only suited to bonded composite where a realistic de-bonded defect can be defined and the loads produce a uniform linear strain regime. The cohesive fracture model addresses some of the limitations of LEFM, such as the material softening at the crack front and the damage initiation of the delamination in monolithic composites. For the fracture mechanics, the sensitivity to mesh shape still exists and will limit the applicability to the impact problems when used in conjunction with current nonadaptive FE methods. The primary advantage of the fracture mechanics methods is that fracture mechanics concepts can be readily incorporated, such as critical energy release rate. However, the adaptation of the fracture mechanics methods to FEA is somewhat more complicated, because it requires that the cracks be explicitly modeled, which in turn affects the discretization scheme.

Recently, the Heaviside step function was introduced into the displacements field in the thickness direction for modeling the delamination. Barbero and Reddy [24] extended the Reddy's layerwise laminate theory to account for multiple delaminations. Delaminations were modeled by jump discontinuous conditions at the interfaces through the thickness direction. At delaminated interfaces, the displacements on adjacent layers remain independent, allowing for separation and slipping. Chattopkdhyay and Gu [25] established a new higher order plate theory for modeling delamination buckling and postbuckling of composite laminates. In both lower and higher order terms of displacements, delaminations between layers of composite plates are modeled by jump discontinuity conditions at the delaminated interfaces. Some higher order terms are identified at the beginning of the formulation by using the conditions that shear stresses vanish at all free surfaces including the delaminated interfaces. Williams [26, 27] presented a generalized multilength scale theory for the laminated plates with delaminations based on a generalized two length scale displacement field assumption obtained from a superposition of global and local displacement effects. By the appropriate simplification, this displacement field can be reduced to any currently available theory, such as the variationally derived, displacements based (discrete layer, smeared, or zig-zag) plate theory. Cho and Kim [28, 29] presented a higher-order zig-zag theory for the laminated composite plates with multiple delaminations by imposing top and bottom surface transverse shear stress-free conditions and interface continuity conditions of transverse shear stresses including delaminated interfaces. The influence of the number, shape, size, and locations of delaminations on the responses can be taken into account systematically by using this displacement field model. In addition, other works [30, 31] introduced the discontinuities into an otherwise continuous solution through well-designed coupling techniques between continuous (differential based) and discontinuous (integral based) solutions.

DOI: 10.1002/nme

Although there are a larger number of works focus on the delamination or matrix cracks problems, only a few studies have been conducted on the problem of the delamination process induced by transverse cracks. O'Brien [32] developed a simple analytical model to estimate the energy release rate associated with the growth of delamination induced by a transverse crack. Dharani and Tang [33] developed a micromechanics analytical model for characterizing the fracture behavior of a fibre reinforced composite laminate containing a transverse matrix crack and longitudinal delaminations along 0/90 interface. In this micromechanics analytical model, a consistent shear lag theory is used to represent the stress-displacement relations. Nairn and Hu [34] extended the variational analysis of transverse cracking developed by Hashin [17, 18] into cross-ply laminates to account for the initiation and growth of delaminations induced by matrix microcracks. For the composite laminate having microcracks and delaminations, a new two-dimensional stress analysis is used to calculate the total strain energy, the effective modulus, and the longitudinal thermal expansion coefficient. Takeda and Ogihara [35] evaluated the stress distribution in cross-ply laminates containing delamination at the tips of transverse cracks by using the replica technique. Berthelot and Corre [36] developed an analytical model to evaluate the stress distributions in cross-ply laminates containing transverse cracks and delamination. In the region without delamination, the analytical approach is reduced to the usual one-dimensional analysis. In the delaminated region, the analytical model is based on a displacement approach in which the longitudinal displacement depends on the longitudinal and transverse coordinates in each layer. Ladeze *et al.* [37, 38] present a relatively complete bridge between the descriptions on the microscales and mesoscales of damaged laminated composites. The coupling between delamination and transverse cracking in laminate structure can be actually simulated. Swindeman [39] developed a method to model coupled matrix cracks and delamination in laminated composite materials and experimentally validated it. In this method, the delamination and the matrix cracks are modeled by using the cohesive zones and a robust mesh-independent cracking technique (regularized extended FEM, Rx-FEM), respectively. In the Rx-FEM, the regularized forms of the Heaviside and Dirac Delta functions are used to transform the crack surface into a volumetric crack zone.

In order to solve the problems that exhibit strong and weak discontinuities in material and geometric behavior, the extended FEM (XFEM) is specifically developed by using the conventional FEM and the concept of partition of unity [40–45]. This method was improved to model in-plane cracks and crack growth in plates and shell [46–49]. For the problem of interface cracks between dissimilar materials, XFEM was extended by the orthotropic enrichment functions [50–56]. For the dynamic crack propagation of composites, Motamedi and Mohammadi [57–59] presented the dynamic crack tip enrichments. Mohammadi and his coworkers [60–62] extended XFEM to fracture analysis of orthotropic functionally graded materials. Recently, XFEM was further extended to the problem of delamination in the composite laminated structures. Nagashima and Suemasu [63] applied XFEM to stress analysis of thin-walled composite laminated plate, which contains an interface delamination. In this method, the nodes on the interface are enriched in order to model the delamination. Curiel Sosa and Karapurath [64] presented an application of the XFEM to the simulation of delamination in fibre metal laminates. This study considers a double cantilever beam made of fibre metal laminate in which crack opens in mode I.

Although the shell elements method improved by XFEM was applied to model thick-through cracks or delaminations individually for the composite laminated structures, there is no work has yet been reported for the typical damage pattern including matrix crack and delamination. It can be seen from Figure 1 that the typical damage pattern of composite laminated structures is a complex three-dimensional crack with layered characteristics. Because it is very difficult to apply XFEM directly to deal with complex three-dimensional crack, we can convert the complex three-dimensional crack with layered characteristics to a one-dimensional crack (matrix cracks) and a two-dimensional crack (delaminations) by using an appropriate displacements model along thickness direction, see Figure 2, assuming that the matrix cracks is perpendicular to the middle surface of each single layer. There are a large number of displacements field along the thickness direction applied to the composite laminated structures [65], such as the equivalent single-layer theory, three-dimensional elasticity theory and multiple model methods. For three-dimensional problems, such as the composite

DOI: 10.1002/nme

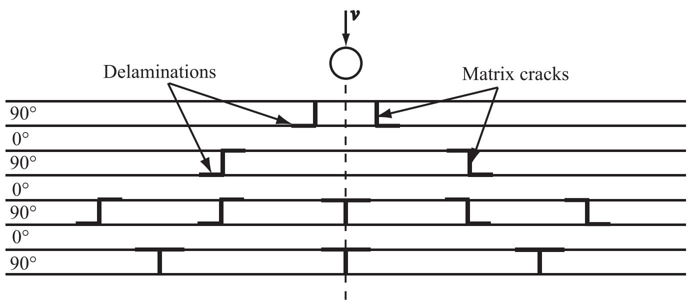

Figure 2. A simplified pattern for typical matrix cracks and delaminations resulted from low impact.

laminated structures with delaminations and cracks, the equivalent single-layer theories are often not sufficiently accurate and often incapable of determining the 3D stress field at the ply level.

In contrast to the equivalent single-layer theory, the layerwise theories are established by assuming that the displacement field exhibits only C0-continuity through the thickness. The layerwise theories can represent the zigzag behavior of the in-plane displacements through the thickness, and providing an effective way to accurately calculate the inplane and transverse stresses. The displacements field employed in Layerwise theories can be used to calculate the three-dimensional stresses and strains of each mathematics layer, particularly the finite element model of the displacement-based full layerwise theory of Reddy is equivalent to the displacement-based finite element model of 3D elasticity [65]. In the layerwise theory of Reddy [66–70], the transverse variations of the displacement components are represented in terms of one-dimensional Lagrangian finite elements. Thus, the displacement components are continuous through the laminate thickness, but the derivatives of the displacements with respect to the thickness coordinate may be discontinuous at various points through the thickness. So the layerwise theory with appropriate improvements is very suitable to simulate the complex three-dimensional crack with layered characteristics together with XFEM.

In this work, an extended layerwise method (XLWM) is established for the composite laminated beams with multiple delaminations and matrix cracks. A new displacement field is proposed in the thickness direction, which contains the linear Lagrange interpolation functions, the one-dimensional weak discontinuous function and strong discontinuous function. The strong and weak discontinuous functions are applied to model the displacement discontinuity induced by delaminations and the strain discontinuity induced by the interface between the layers, respectively. Because the nodes in the thickness direction are located at the middle surface of each single layer, the in-plane matrix cracks can be modeled conveniently by employing the XFEM in the in-plane discrete scheme. Therefore, the XLWM has the capability to model the composite laminated beams with multiple delaminations and matrix cracks.

The rest of the paper is organized as follows. In the next section, a new displacement field along the thickness direction is proposed for the composite laminated beam. The in-plane displacement approximation used to model the composite laminated beam with multiple delaminations and/or matrix cracks is described as well. In Sections 3 and 4, the Hamilton's principle, Euler–Lagrange equations and constitutive equations are established for the XLWM. The governing equations for multiple delaminations and/or matrix cracks are developed in Section 5. In order to demonstrate the excellent predictive capability of the XLWM method, static analysis for several composite laminated beams with multiple matrix cracks and/or delaminations is investigated in Section 6. Finally, some conclusions are drawn in Section 7.

2. DISPLACEMENTS FIELD

2.1. *Displacements field along the thickness direction*

In order to model the displacement discontinuity of delaminations based on the strong discontinuous functions, the nodes of the displacements field along the thickness direction should be located at the top surface, the bottom surface, and the middle surface of each single layer. This node strategy

DOI: 10.1002/nme

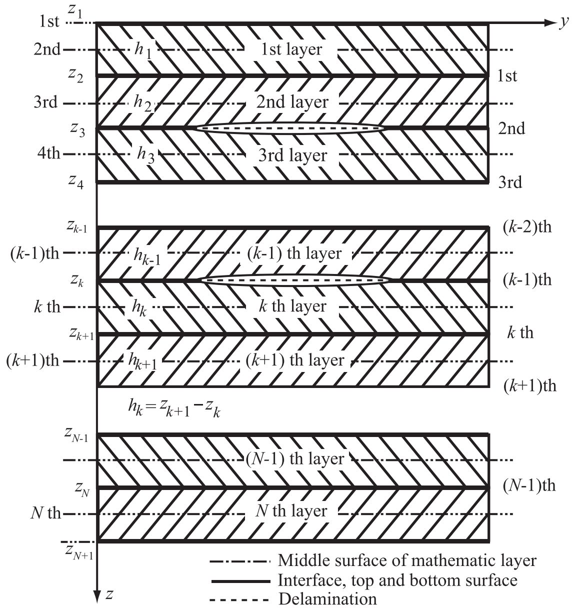

Figure 3. Displacements field for the composite laminated beam with multiple delaminations.

is also necessary for the simulation of in-plane matrix cracks. However, the weak discontinuous function is needed in this displacements field to model the strain discontinuity resulted from the interfaces between the layers. For the composite laminated beam with multiple delaminations, the displacements field proposed in the present work is schematically shown in Figure 3, where h_k is the thickness of the k-th layer and z_k is the coordinate of the interface between k-th layer and $(k-1)$-th layer in thickness direction. In Figure 3, the numbers on the left side denote the nodes of the displacements field along the thickness direction, while the numbers on the right side denote the interfaces between the layers.

The displacements at point (y, z) in the composite laminated beam with multiple delaminations can be expressed as

$$u_\alpha(y,z,t) = \sum_{k=1}^{N+2} \phi_k(z) u_{\alpha ik}(y,t) + \sum_{k=1}^{N_D} \Xi_k(z) u_{\alpha lk}(y,t) + \sum_{k=1}^{N} \Theta_k(z) u_{\alpha rk}(y,t) \qquad (1)$$

where $\alpha = 1, 2$ denotes the components in y and z directions. $u_{\alpha ik}$, $u_{\alpha lk}$, and $u_{\alpha rk}$ are the nodal freedoms, the additional nodal freedoms to model displacement discontinuities induced by delaminations, and the additional nodal freedoms to model strain discontinuities induced by interfaces between the layers, respectively. The subscripts i, l, and r denote the standard nodal freedom, the additional nodal freedom for delaminations, and the additional nodal freedom for interfaces, respectively. ϕ_k is the linear Lagrange interpolation functions along the thickness direction of the composite laminated beam, see Figure 4(a). $\Theta_k = \phi_k(z)\chi_k(z)$ is the weak discontinuous shape function used to model the strains discontinuity in the interface between the layers, see Figure 4(b), where $\chi_k(z)$ is the one-dimensional signed distance function. $\Xi_k = \phi_k(z)H_k(z)$ is the shape function used to model delaminations, see Figure 4(c), where $H_k(z)$ is the one-dimensional Heaviside function. N is the number of the mathematical layers of the composite laminated beam. It can be seen from Figure 3 that the numbers of the standard freedoms and the additional freedoms for interfaces are $N+2$ and N, respectively. N_D is the number of nodes that have to be enriched to model the delaminations.

DOI: 10.1002/nme

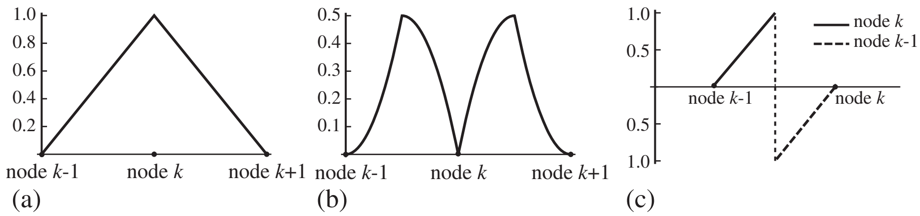

Figure 4. Shape functions in the displacement field. (a) ϕ_k ; (b) $\Theta_k = \phi_k(z)\chi_k(z)$; (c) $\Xi_k = \phi_k(z)H_k(z)$.

The linear Lagrange interpolation functions ϕ_k can be expressed as

$$\phi_k(z) = \begin{cases} \varphi_k^1 = \frac{\bar{z}_{k-1}-z}{\bar{z}_k-\bar{z}_{k-1}} & \bar{z}_{k-1} \leqslant z \leqslant \bar{z}_k \\ \varphi_k^2 = \frac{z-\bar{z}_{k+1}}{\bar{z}_{k+1}-\bar{z}_k} & \bar{z}_k \leqslant z \leqslant \bar{z}_{k+1} \end{cases} \tag{2}$$

where $\bar{z}_0 = z_1$, $\bar{z}_1 = \frac{z_1+z_2}{2}, \cdots, \bar{z}_k = \frac{z_k+z_{k+1}}{2}, \cdots \bar{z}_N = \frac{z_N+z_{N+1}}{2}$, $\bar{z}_{N+1} = z_{N+1}$. z_k are defined in Figure 3.

The weak discontinuous shape function Θ_k can be expressed as

$$\Theta_k = \begin{cases} \varphi_k^1 \frac{\bar{z}_{k-1}-z}{\bar{z}_{k-1}-z_{k-1}} & \bar{z}_{k-1} \leqslant z \leqslant z_k \\ \varphi_k^1 \frac{z-\bar{z}_k}{\bar{z}_k-z_k} & z_k \leqslant z \leqslant \bar{z}_k \\ \varphi_k^2 \frac{\bar{z}_k-z}{\bar{z}_k-z_k} & \bar{z}_k \leqslant z \leqslant z_{k+1} \\ \varphi_k^2 \frac{z-\bar{z}_{k+1}}{\bar{z}_{k+1}-z_{k+1}} & z_{k+1} \leqslant z \leqslant \bar{z}_{k+1} \end{cases} \tag{3}$$

The shape function Ξ_k used to model delaminations can be expressed as

$$\Xi_k = \begin{cases} \frac{\bar{z}_{k-1}-z}{\bar{z}_{k-1}-z_{k-1}} & z_k \leqslant z \leqslant \bar{z}_k \\ \frac{z-\bar{z}_{k+1}}{\bar{z}_{k+1}-z_{k+1}} & \bar{z}_k \leqslant z \leqslant z_{k+1} \end{cases} \tag{4}$$

The present layerwise concept is very general in that the number of subdivisions (mathematical layers) can be greater than, equal to, or less than the number of the material layers through the thickness direction. A mathematical layer is represented as an equivalent, single, and homogeneous layer. If there are continuous and uniform stacking sequences in composite laminated structures, the computational cost of the layerwise theories can be reduced significantly by using the sublaminate concept, which makes the number of mathematical layers much less than the number of the material layers.

Let

$$\Phi_{ik} = \phi_k(z), \Phi_{lk} = \Xi_k(z), \Phi_{rk} = \Theta_k(z) \tag{5}$$

Equation (1) can be simplified as

$$u_\alpha = \Phi_{\zeta k} u_{\alpha\zeta k}, \zeta = i, l, r \tag{6}$$

where the Einstein summation convention is used, namely, the repeated indexes k and ζ imply summation over all its values. The values of k depend on the value of ζ, see Equation (1). For example, k takes value from 1 to $N+2$ when ζ equals to i, but takes value from 1 to N when ζ equals to r. If there is no delaminations in the thickness direction, ζ in Equation (6) takes value of i and r only.

In the displacement-based full layerwise of Reddy [65], the layerwise continuous functions, such as the one-dimensional Lagrange interpolation functions along the thickness direction, are used to develop the displacement field of the composite laminated structures. Because the nodes of the interpolation functions along the thickness direction are located at the surfaces and the interfaces between the layers, the displacement components are continuous through the thickness direction, but the derivatives of the displacements (strains) are discontinuous at the interfaces. Therefore, the displacements field present here can be viewed as an improvement and extension to the Reddy's theory.

2.2. *In-plane displacements discretization*

Because the nodes in the thickness direction are located at the middle surface of each single layer, the in-plane matrix cracks can be modeled conveniently by employing the XFEM in the extend layerwise method. Therefore, the basic idea of the present method is to convert a complex three-dimensional fracture problem to a one-dimensional and a two-dimensional fracture problem. For the composite laminated beam with multiple delaminations and matrix cracks, the nodal displacements and addition freedoms $u_{\alpha\zeta k}$ $(\zeta = i, l, r)$ are expressed over each element as a linear combination of the one-dimensional Lagrange interpolation function ψ_m and a one-dimensional discontinuous enrichment function as

$$u_{\alpha\zeta k}(y,t) = \psi_m(y)U_{\alpha\zeta km}(t) + \Lambda_s(y)\bar{U}_{\alpha\zeta ks}(t) \tag{7}$$

where $m = 1, \cdots, N_E$ is the number of in-plane finite element nodes and $U_{\alpha\zeta km}$ is the nodal value of in-plane finite element nodes. $s = 1, \cdots, N_E^P$ is the number of in-plane enriched nodes, which are affected by the in-plane cracks, $\bar{U}_{\alpha iks}$, $\bar{U}_{\alpha lks}$, and $\bar{U}_{\alpha rks}$ are the additional freedoms introduced by the in-plane matrix cracks. $\Lambda_s = \psi_s(y)H_s(y)$ is the shape function used to model the in-plane cracks, see Figure 5, where $H_s(y)$ is the Heaviside function. If the XLWM is extended to the composite laminated plates/shells with multiple delaminations and in-plane matrix cracks, the additional freedoms need to be added into Equation (7) to model the tip of the in-plane matrix cracks.

As shown in Figure 1, the tips of the matrix cracks are often located at the interface. Because the nodes in the thickness direction are located at the middle surface of each single layer, the tip of mathematics matrix crack in the XLWM is located at the middle surface, instead of the interface,

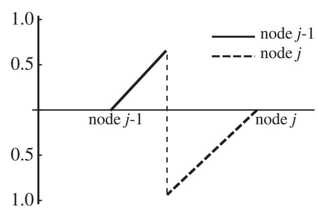

Figure 5. Shape function Λ_s.

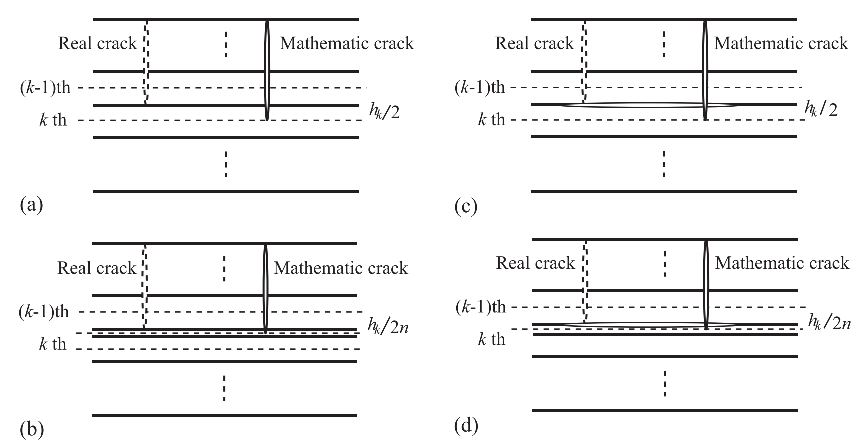

Figure 6. Location of the tip of real and mathematical matrix crack.

DOI: 10.1002/nme

see Figure 6(a) and (c). Therefore, the mathematical crack in XLWM is $h_k/2$ longer than that of the real crack. In order to better model the tip of a real crack, which is often located at the interface, we can divide the single layer near the tip of the real crack into two sublayers, see Figure 6(b) and (d). Assuming that the thickness of the sublayer near the tip of real crack is h_k/n, the mathematical crack is just $h_k/2n$ longer than that of the real crack, instead of $h_k/2$.

For the composite laminated beam with multiple delaminations only, the node displacements and the addition freedoms in the extend layerwise method can be expressed over each element as a linear combination of the one-dimensional Lagrange interpolation function ψ_m as follows:

$$u_{\alpha\zeta k}(y,t) = \psi_m(y) U_{\alpha\zeta km}(t) \tag{8}$$

where $m = 1, \cdots, N_E$ is the number of in-plane finite element nodes, and $U_{\alpha\zeta km}$ is the nodal value of in-plane finite element nodes.

3. HAMILTON'S PRINCIPLE AND EULER–LAGRANGE EQUATIONS

Substituting the displacements field Equation (6) into the strain-displacement relationship results in

$$\begin{aligned} \varepsilon_{yy} &= \Phi_{\zeta k} u_{1\zeta k,y} \\ \varepsilon_{yz} &= \Phi_{\zeta k,z} u_{1\zeta k} + \Phi_{\zeta k} u_{2\zeta k,y} \\ \varepsilon_{zz} &= \Phi_{\zeta k,z} u_{2\zeta k} \end{aligned} \tag{9}$$

where the subscript (,) denotes differential operation.

Hamilton's principle [65] is employed to derive the equations of motion for the composite laminated beam with multiple delaminations. Using the first order variation of strain, which can be obtained from Equation (9), the virtual strain energy for the present problem is given by

$$\begin{aligned} \delta U &= \int_L \int_{-\frac{H}{2}}^{\frac{H}{2}} \left(\sigma_{yy}\delta\varepsilon_{yy} + \sigma_{zz}\delta\varepsilon_{zz} + \sigma_{yz}\delta\varepsilon_{yz}\right) dz dy \\ &= \int_L \left(N_{\zeta k}^{y} \delta u_{1\zeta k,y} + Q_{\zeta k}^{yz} \delta u_{1\zeta k} + N_{\zeta k}^{yz} \delta u_{2\zeta k,y} + Q_{\zeta k}^{zz} \delta u_{2\zeta k}\right) dy \end{aligned} \tag{10}$$

where H is the thickness of the composite laminated beams. The stress resultants in Equation (10) are given by

$$\begin{aligned} \left(N_{\zeta k}^{y}, N_{\zeta k}^{yz}\right) &= \int_{-\frac{H}{2}}^{\frac{H}{2}} \left(\sigma_{yy}, \sigma_{yz}\right) \Phi_{\zeta k} dz, \\ \left(Q_{\zeta k}^{yz}, Q_{\zeta k}^{zz}\right) &= \int_{-\frac{H}{2}}^{\frac{H}{2}} \left(\sigma_{yz}, \sigma_{zz}\right) \Phi_{\zeta k,z} dz \end{aligned} \tag{11}$$

The virtual work carried out by applied forces is given by

$$\begin{aligned} \delta V &= -\int_L \left[q_b(y,t)\delta u_2\left(y, -\frac{H}{2}, t\right) + q_t(y,t)\delta u_2\left(y, \frac{H}{2}, t\right)\right] dy \\ &= -\int_L \left(q_b \delta u_2^{N+1} + q_t \delta u_2^{0}\right) dy \end{aligned} \tag{12}$$

where $q_b(y,t)$ and $q_t(y,t)$ are the distributed force at the bottom surface $\left(z = -\frac{H}{2}\right)$ and the top surface $\left(z = \frac{H}{2}\right)$ of the laminated beam, respectively.

DOI: 10.1002/nme

The variation of kinetic energy is given by

$$\begin{aligned}\delta M &= \int_L \int_{-\frac{H}{2}}^{\frac{H}{2}} \rho_0 \left(\dot{u}_1 \delta \dot{u}_1 + \dot{u}_2 \delta \dot{u}_2\right) dz dy \\ &= \int_L \int_{-\frac{H}{2}}^{\frac{H}{2}} \rho_0 \left(\Phi_{\zeta k} \Phi_{\eta e} \dot{u}_{1\eta e} \delta \dot{u}_{1\zeta k} + \Phi_{\zeta k} \Phi_{\eta e} \dot{u}_{2\eta e} \delta \dot{u}_{2\zeta k}\right) dz dy \\ &= \int_L \left(I_{\zeta\eta k e} \dot{u}_{1\eta e} \delta \dot{u}_{1\zeta k} + I_{\zeta\eta k e} \dot{u}_{2\eta e} \delta \dot{u}_{2\zeta k}\right) dy\end{aligned} \tag{13}$$

where

$$I_{\zeta\eta k e} = \int_{-\frac{H}{2}}^{\frac{H}{2}} \rho_0 \Phi_{\zeta k} \Phi_{\eta e} dz \tag{14}$$

Substituting Equations (10), (12), and (13) into the Hamilton's principle [65], and integrating by parts, leads to

$$\begin{aligned}\int_0^T (\delta U + \delta V - \delta M)\mathrm{d}t = \int_0^T \Bigg[& N_{\zeta k}^{y} \delta u_{1\zeta k}|_{\Gamma_\sigma} + N_{\zeta k}^{yz} \delta u_{2\zeta k}|_{\Gamma_\sigma} \\ & - \int_L \Big(N_{\zeta k,y}^{y} \delta u_{1\zeta k} - Q_{\zeta k}^{yz} \delta u_{1\zeta k} \\ & + N_{\zeta k,y}^{yz} \delta u_{2\zeta k} - Q_{\zeta k}^{zz} \delta u_{2\zeta k} \Big) \mathrm{d}y \\ & + \int_L \left(I_{\zeta\eta k e} \ddot{u}_{1\eta e} \delta u_{1\zeta k} + I_{\zeta\eta k e} \ddot{u}_{2\eta e} \delta u_{2\zeta k} \right) \mathrm{d}y \\ & - \int_L \left(q_b \delta u_2^{N+1} + q_t \delta u_2^0 \right) \mathrm{d}y \Bigg] \mathrm{d}t = 0\end{aligned} \tag{15}$$

where δU is the virtual strain energy. δV is the virtual work carried out by applied forces. δM is the virtual kinetic energy.

From the Hamilton's principle Equation (15), the Euler–Lagrange equations of the composite laminated beam with multiple delaminations, which contain $2\left[(N+2) + N + N_D\right]$ equations, can be obtained as

$$\begin{aligned}\delta u_{1\zeta k} &: N_{\zeta k,y}^{y} - Q_{\zeta k}^{yz} = I_{\zeta\eta k e} \ddot{u}_{1\eta e} \\ \delta u_{2\zeta k} &: N_{\zeta k,y}^{yz} - Q_{\zeta k}^{zz} + q_b \delta_k^{N+1} + q_t \delta_k^0 = I_{\zeta\eta k e} \ddot{u}_{2\eta e}\end{aligned} \tag{16}$$

with natural boundary conditions

$$\begin{aligned}\delta u_{1\zeta k} &: N_{\zeta k}^{y}|_{\Gamma_\sigma} = 0 \\ \delta u_{2\zeta k} &: N_{\zeta k}^{yz}|_{\Gamma_\sigma} = 0\end{aligned} \tag{17}$$

4. CONSTITUTIVE EQUATIONS

Assume that the beam is laminated of orthotropic laminates with arbitrary fiber direction in the x-y plane with respect to the y-axis. The constitutive law of the μ-th lamina with respect to the global

DOI: 10.1002/nme

x-y-z coordinate system is

$$\begin{Bmatrix} \sigma_{xx} \\ \sigma_{yy} \\ \sigma_{zz} \\ \sigma_{yz} \\ \sigma_{xz} \\ \sigma_{xy} \end{Bmatrix}^{(\mu)} = \begin{bmatrix} C_{11} & C_{12} & C_{13} & 0 & 0 & C_{16} \\ C_{12} & C_{22} & C_{11} & 0 & 0 & C_{26} \\ C_{13} & C_{23} & C_{33} & 0 & 0 & C_{36} \\ 0 & 0 & 0 & C_{44} & C_{45} & 0 \\ 0 & 0 & 0 & C_{45} & C_{55} & 0 \\ C_{16} & C_{26} & C_{36} & 0 & 0 & C_{66} \end{bmatrix}^{(\mu)} \begin{Bmatrix} \varepsilon_{xx} \\ \varepsilon_{yy} \\ \varepsilon_{zz} \\ \varepsilon_{yz} \\ \varepsilon_{xz} \\ \varepsilon_{xy} \end{Bmatrix}^{(\mu)} \tag{18}$$

For the beam problem, the three-dimensional constitutive equations can be reduced to a two-dimensional form by eliminating the normal stress σ_{xx}, the shear stress σ_{xy}, and the transverse shear stress σ_{xz}. Thus, the constitutive equations of composite laminated beam are obtained as

$$\begin{Bmatrix} \sigma_{yy} \\ \sigma_{zz} \\ \sigma_{yz} \end{Bmatrix}^{(\mu)} = \begin{bmatrix} \bar{C}_{11} & \bar{C}_{13} & 0 \\ \bar{C}_{13} & \bar{C}_{33} & 0 \\ 0 & 0 & \bar{C}_{44} \end{bmatrix}^{(\mu)} \begin{Bmatrix} \varepsilon_{yy} \\ \varepsilon_{zz} \\ \varepsilon_{yz} \end{Bmatrix}^{(\mu)} \tag{19}$$

where

$$\begin{aligned} \begin{bmatrix} \bar{C}_{11} & \bar{C}_{13} & 0 \\ \bar{C}_{13} & \bar{C}_{33} & 0 \\ 0 & 0 & \bar{C}_{44} \end{bmatrix}^{(\mu)} &= \begin{bmatrix} C_{11} & C_{13} & 0 \\ C_{13} & C_{33} & 0 \\ 0 & 0 & C_{55} \end{bmatrix}^{(\mu)} \\ &- \begin{bmatrix} C_{12} & 0 & C_{16} \\ C_{23} & 0 & C_{36} \\ 0 & C_{45} & 0 \end{bmatrix}^{(\mu)} \left(\begin{bmatrix} C_{22} & 0 & C_{26} \\ 0 & C_{44} & 0 \\ C_{26} & 0 & C_{66} \end{bmatrix}^{(\mu)} \right)^{-1} \begin{bmatrix} C_{12} & C_{23} & 0 \\ 0 & 0 & C_{45} \\ C_{16} & C_{36} & 0 \end{bmatrix}^{(\mu)} \end{aligned} \tag{20}$$

Substituting the constitutive Equation (20) into the stress resultants Equation (11) leads to

$$N_{\zeta k}^{y} = \int_{-\frac{H}{2}}^{\frac{H}{2}} (\bar{C}_{11}\varepsilon_{yy} + \bar{C}_{13}\varepsilon_{zz})\Phi_{\zeta k} dz = A^{1}_{11\zeta\eta ke} u_{1\eta e,y} + A^{2}_{13\zeta\eta ke} u_{2\eta e} \tag{21}$$

$$Q_{\zeta k}^{yz} = \int_{-\frac{H}{2}}^{\frac{H}{2}} (\bar{C}_{44}\varepsilon_{yz})\Phi_{\zeta k,z} dz = A^{4}_{44\zeta\eta ke} u_{1\eta e} + A^{3}_{44\zeta\eta ke} u_{2\eta e,y} \tag{22}$$

$$N_{\zeta k}^{yz} = \int_{-\frac{H}{2}}^{\frac{H}{2}} (\bar{C}_{44}\varepsilon_{yz})\Phi_{\zeta k} dz = A^{2}_{44\zeta\eta ke} u_{1\eta e} + A^{1}_{44\zeta\eta ke} u_{2\eta e,y} \tag{23}$$

$$Q_{\zeta k}^{zz} = \int_{-\frac{H}{2}}^{\frac{H}{2}} (\bar{C}_{13}\varepsilon_{yy} + \bar{C}_{33}\varepsilon_{zz})\Phi_{\zeta k,z} dz = A^{3}_{13\zeta\eta ke} u_{1\eta e,y} + A^{4}_{33\zeta\eta ke} u_{2\eta e} \tag{24}$$

where the laminate stiffness coefficients $A^{1}_{pq\zeta\eta ke}$, $A^{2}_{pq\zeta\eta ke}$, $A^{3}_{pq\zeta\eta ke}$, and $A^{4}_{pq\zeta\eta ke}$ are given in terms of the modified elastic constants and the through-thickness interpolation polynomials as

$$\begin{aligned} A^{1}_{pq\zeta\eta ke} &= \int_{-\frac{H}{2}}^{\frac{H}{2}} \Phi_{\zeta k} \bar{C}_{pq} \Phi_{\eta e} dz, \\ A^{2}_{pq\zeta\eta ke} &= \int_{-\frac{H}{2}}^{\frac{H}{2}} \Phi_{\zeta k,z} \bar{C}_{pq} \Phi_{\eta e} dz, \\ A^{3}_{pq\zeta\eta ke} &= \int_{-\frac{H}{2}}^{\frac{H}{2}} \Phi_{\zeta k} \bar{C}_{pq} \Phi_{\eta e,z} dz, \\ A^{4}_{pq\zeta\eta ke} &= \int_{-\frac{H}{2}}^{\frac{H}{2}} \Phi_{\zeta k,z} \bar{C}_{pq} \Phi_{\eta e,z} dz, \end{aligned} \qquad p,q = 1,3,4 \tag{25}$$

DOI: 10.1002/nme

5. GOVERNING EQUATIONS

5.1. Governing equations for multiple delaminations

Substituting Equations (8) into (15), for static problem, results in the finite element formulation of the composite laminated beam with multiple delaminations as

$$\boldsymbol{K}_{\zeta\eta kemn}\boldsymbol{U}_{\eta en} = \boldsymbol{F}_{\zeta km} \tag{26}$$

where $m, n = 1, \cdots, N_E$; $\boldsymbol{K}_{\zeta\eta kemn}$ is the element stiffness matrix given by

$$\boldsymbol{K}_{\zeta\eta kemn} = \begin{bmatrix} \psi_{m,y}A^1_{11\zeta\eta ke}\psi_{n,y} + \psi_m A^4_{44\zeta\eta ke}\psi_n & \psi_{m,y}A^2_{13\zeta\eta ke}\psi_n + \psi_m A^3_{44\zeta\eta ke}\psi_{n,y} \\ \psi_{m,y}A^2_{44\zeta\eta ke}\psi_n + \psi_m A^3_{13\zeta\eta ke}\psi_{n,y} & \psi_{m,y}A^1_{44\zeta\eta ke}\psi_{n,y} + \psi_m A^4_{33\zeta\eta ke}\psi_n \end{bmatrix} \tag{27}$$

It can be seen from Equation (27) that for the composite laminated beam with multiple delaminations the submatrices of the element stiffness matrix in the extend layerwise method have the same form with the element stiffness matrix of the layerwise method developed by Reddy [71]. However, the laminate stiffness coefficients in Equation (25) are not different with that in Reddy's layerwise method.

5.2. Governing equations for multiple delaminations and matrix cracks

For static problem, substituting Equation (7) into (15) leads to the finite element formulation of the composite laminated beam with multiple delaminations and matrix cracks as

$$\boldsymbol{K}_{\zeta\eta ke\kappa\iota}\boldsymbol{U}_{\eta e\iota} = \boldsymbol{F}_{\zeta k\kappa} \tag{28}$$

where $\kappa = m, s$; $\iota = n, g$; $m, n = 1, 2, \cdots N_E$; $s, g = 1, \cdots N_E^P$; $\boldsymbol{K}_{\zeta\eta ke\kappa\iota}$ is the element stiffness matrix given by

$$\boldsymbol{K}_{\zeta\eta kemg} = \begin{bmatrix} \psi_{m,y}A^1_{11\zeta\eta ke}\Lambda_{g,y} + \psi_m A^4_{44\zeta\eta ke}\Lambda_g & \psi_{m,y}A^2_{13\zeta\eta ke}\Lambda_g + \psi_m A^3_{44\zeta\eta ke}\Lambda_{g,y} \\ \psi_{m,y}A^2_{44\zeta\eta ke}\Lambda_g + \psi_m A^3_{13\zeta\eta ke}\Lambda_{g,y} & \psi_{m,y}A^1_{44\zeta\eta ke}\Lambda_{g,y} + \psi_m A^4_{33\zeta\eta ke}\Lambda_g \end{bmatrix} \tag{29}$$

$$\boldsymbol{K}_{\zeta\eta kesn} = \begin{bmatrix} \Lambda_{s,y}A^1_{11\zeta\eta ke}\psi_{n,y} + \Lambda_s A^4_{44\zeta\eta ke}\psi_n & \Lambda_{s,y}A^2_{13\zeta\eta ke}\psi_n + \Lambda_s A^3_{44\zeta\eta ke}\psi_{n,y} \\ \Lambda_{s,y}A^2_{44\zeta\eta ke}\psi_n + \Lambda_s A^3_{13\zeta\eta ke}\psi_{n,y} & \Lambda_{s,y}A^1_{44\zeta\eta ke}\psi_{n,y} + \Lambda_s A^4_{33\zeta\eta ke}\psi_n \end{bmatrix} \tag{30}$$

$$\boldsymbol{K}_{\zeta\eta kesg} = \begin{bmatrix} \Lambda_{s,y}A^1_{11\zeta\eta ke}\Lambda_{g,y} + \Lambda_s A^4_{44\zeta\eta ke}\Lambda_g & \Lambda_{s,y}A^2_{13\zeta\eta ke}\Lambda_g + \Lambda_s A^3_{44\zeta\eta ke}\Lambda_{g,y} \\ \Lambda_{s,y}A^2_{44\zeta\eta ke}\Lambda_g + \Lambda_s A^3_{13\zeta\eta ke}\Lambda_{g,y} & \Lambda_{s,y}A^1_{44\zeta\eta ke}\Lambda_{g,y} + \Lambda_s A^4_{33\zeta\eta ke}\Lambda_g \end{bmatrix} \tag{31}$$

For the composite laminated beam with multiple delaminations and matrix cracks, it can be seen from Equations (29–31) that the submatrices of the element stiffness matrix in the extend layerwise method is composed of four submatrices. $\boldsymbol{K}_{\zeta\eta kemn}$ and $\boldsymbol{K}_{\zeta\eta kesg}$ are the submatrices of the nodal freedoms and the additional nodal freedoms, respectively. $\boldsymbol{K}_{\zeta\eta kemg}$ and $\boldsymbol{K}_{\zeta\eta kesn}$ are the coupling submatrices of the nodal freedoms and the additional nodal freedoms. These four submatrices have the same form with the element stiffness matrix of the layerwise method developed by Reddy [71].

6. NUMERICAL EXAMPLES

6.1. Composite laminated beam without damages

The composite laminated beams without damage are considered in this numerical example. Because the addition freedoms $u_{\alpha lk}$ used to simulate delaminations vanish, the indices ζ and η in Equation (26) only take value of i and r, and the values of k and e depend on the value of ζ, see Equation (1).

DOI: 10.1002/nme

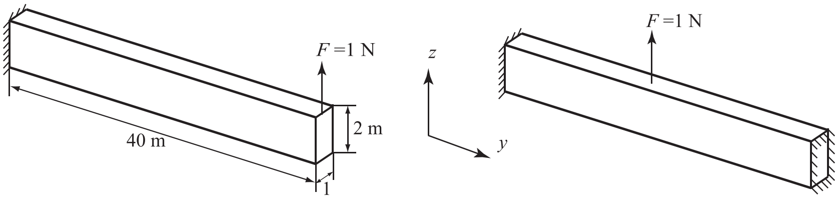

(a) CF (b) CC

Figure 7. Composite laminated beams without damages. (a) one end clamp beam (CF); (b) doubly-clamp beam (CC).

Table I. Maximum displacements obtained by Reddy's Layerwise theory and the XLW method.

	CF				CC			
	u_1 ($10^{-5}m$)		u_2 ($10^{-4}m$)		u_1 ($10^{-7}m$)		u_2 ($10^{-5}m$)	
	LW	XLWM	LW	XLWM	LW	XLWM	LW	XLWM
2 Ele. (5 nodes)	3.00185	3.00242	7.56014	7.56158	0.85294	0.85303	0.13899	0.39000
4 Ele. (9 nodes)	3.00167	3.00215	7.92479	7.92601	9.42912	9.44562	1.05667	1.05801
8 Ele. (17 nodes)	3.00145	3.00181	8.00036	8.00103	9.41905	9.43285	1.25029	1.25161
16 Ele. (33 nodes)	3.00206	3.00251	8.01092	8.01142	9.39910	9.40742	1.27789	1.27907
Euler beam theory			8.0					

XLWM, extended layerwise method; LW, layerwise; CF, one end clamp beam; CC, doubly-clamp beam.

The size, the load cases, and the boundary conditions of the composite beam employed in this example are shown in Figure 7. There are two kinds of boundary conditions, one end clamp (CF) and doubly-clamp (CC).

An isotropic beam is used to validate the proposed method. The isotropic beam is divided into four sublayers, whose material properties are taken as $E = 4 \times 10^4$MPa, $v = 0.3$. Table I and Figure 8 compare the maximum displacements and the deformation pattern of the isotropic beam, respectively, obtained by the proposed XLWM, Reddy's Layerwise theory and Euler beam theory. The magnification of the displacements in the deformation pattern of this example and the following examples is $3.0/\max(u_2)$. It can be seen from Table I that the present method is accurate and reliable for the beams without delamination and in-plane cracks. In addition, the present results are slightly larger than that of Reddy's Layerwise theory, because the number of the nodes along the thickness direction for the present method is more than that of Reddy's Layerwise theory.

The XLWM is also employed to model the cross-ply laminated beam with six elastic layers. The size, the load cases, and the boundary conditions are shown in Figure 7. All the layers have the same thickness and material properties. The material properties of a single layer are taken as $E_{11} = 1.81 \times 10^5$MPa, $E_{22} = E_{33} = 1.03 \times 10^4$KPa, $G_{12} = G_{13} = 7.17 \times 10^3$MPa, $G_{23} = 6.21 \times 10^3$MPa, $G_{12} = 0.28$, $G_{13} = 0.02$, and $G_{23} = 0.40$.

Table II compares the maximum displacements obtained by the proposed XLW method and Reddy's Layerwise theory for the cross-ply laminated beams with different stacking sequences, which shows that the proposed method is also accurate and reliable for the cross-ply laminated beams.

6.2. *Composite laminated beam with multiple delaminations*

In this example, the XLWM is used to model the composite laminated beams with multiple delaminations. The size, the load case, the boundary condition, and the discretization schemes of the composite beam with delamination are shown in Figure 9, together with the size and location of the delamination. Two kinds of boundary conditions, CF and CC, are studied. There are three kinds of stacking sequences: $[0]_8$, $[0/90/0/90]_s$, and $[90/0/90/0]_s$. The material properties of each single layer are taken as $E_{11} = 1.81 \times 10^5$MPa, $E_{22} = E_{33} = 1.03 \times 10^4$MPa, $G_{12} = G_{13} = 7.17 \times 10^3$MPa, $G_{23} = 6.21 \times 10^3$MPa, $G_{12} = 0.28$, and $G_{13} = 0.02$, $G_{23} = 0.40$. In order to

DOI: 10.1002/nme

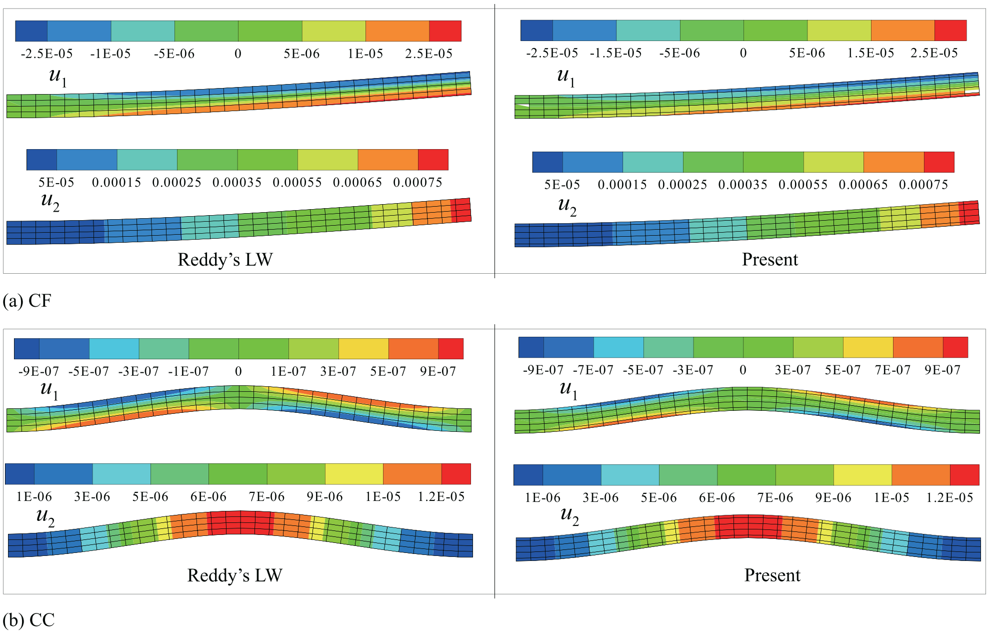

Figure 8. Deformation pattern obtained by present method and Reddy's Layerwise theory. (a) one end clamp beam (CF); (b) doubly-clamp beam (CC).

Table II. Maximum displacements for the composite laminated beams.

	CF				CC			
	u_1 $(10^{-6}m)$		u_2 $(10^{-4}m)$		u_1 $(10^{-7}m)$		u_2 $(10^{-6}m)$	
	LW	XLWM	LW	XLWM	LW	XLWM	LW	XLWM
$[0]_6$	6.67219	6.67878	1.80237	1.80301	2.13246	2.13985	3.64261	3.65843
$[0/90/0]_s$	8.81100	8.81737	2.37405	2.37486	2.77654	2.78673	4.52997	4.54978
$[0/0/90]_s$	6.91140	6.91800	1.86863	1.86925	2.21097	2.21885	3.79713	3.81269
$[90/0/0]_s$	19.8391	19.8483	5.30265	5.30431	6.37617	6.39798	9.37764	9.41769
$[0/90/90]_s$	9.23314	9.23923	2.48939	2.49021	2.90995	2.92068	4.75319	4.77363
$[90/90/0]_s$	72.3246	72.3284	19.2956	19.2987	22.7792	22.8184	31.1946	31.2572
$[90/0/90]_s$	22.1225	22.1327	5.91451	5.91627	7.09253	7.11614	1.03963	1.04396

XLWM, extended layerwise method; LW, layerwise; CF, one end clamp beam; CC, doubly-clamp beam.

validate the proposed XLW method, this problem is also analyzed using MSC.Nastran with Hex8 solid elements, in which nodes pair along the interface are employed to model the delamination. The discretization scheme of the present method is the same with that used in the finite element analysis. The delamination can be denoted as $[\theta/\theta/\theta/\theta/\cap/\theta/\theta/\theta/\theta]$ in the damage region, which means that the delamination is located at the interface between 4th layer and 5th layer.

The maximum displacements obtained by the FEM analysis and the present method for the laminated beams with delamination in the middle of the span for CF and CC boundary conditions are compared in Tables III and IV, respectively. In the XLWM column, the results in brackets are obtained by 2-node elements, while the remaining results are obtained by 3-node elements. It can be seen from Tables III and IV that the increase of the maximum displacement is less than 1% as the number of the nodes increased from 79 to 101. For different element type, reasonable converged values have been achieved, but the convergence rate of 3-node elements is higher than that of 2-node elements. The maximum displacement obtained by 3-node elements are slightly larger than that of 2-node elements. The most important reasons is that this example is a bending problem, and the shape function of the 3-node elements have bending modal. The deformation patterns obtained by the present method for composite beam with delamination are shown in Figure 10, where the

DOI: 10.1002/nme

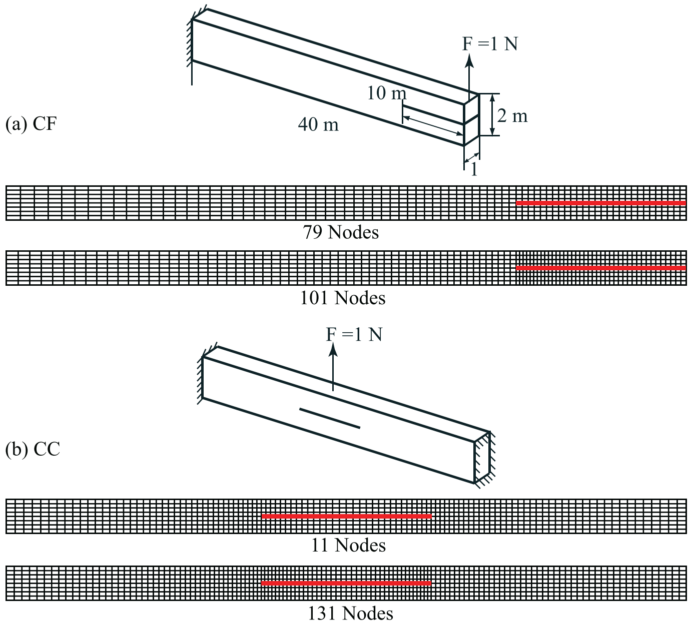

Figure 9. Composite laminated beam with delamination. (a) one end clamp beam (CF); (b) doubly-clamp beam (CC).

Table III. Maximum displacements for the composite laminated beam with delamination at the free end (CF).

		u_1 $(10^{-5}m)$		u_2 $(10^{-4}m)$	
Stacking sequences	Number of nodes	MSC	XLWM	MSC	XLWM
$[0]_8$	79	8.25315	8.28552 (8.23609)	2.07623	2.08307 (2.07139)
	101	8.25848	8.29079 (8.25698)	2.07725	2.08383 (2.07076)
$[0/90/0/90]_s$	79	1.21638	1.22722 (1.21660)	3.13409	3.16742 (3.14017)
	101	1.21695	1.22829 (1.22157)	3.13544	3.17020 (3.15293)
$[90/0/90/0]_s$	79	2.29316	2.31304 (2.28079)	5.59327	5.61992 (5.54563)
	101	2.29477	2.31551 (2.29282)	5.59542	5.62149 (5.57115)

XLWM, extended layerwise method; MSC, finite element analysis code MSC.Patran/Nastran.

stacking sequence is $[0]_8$. It is obvious that the maximum values and the fringes of the displacements obtained by present method are in good agreement with those of MSC.Nastran.

Figure 11 presents the comparison of the stresses σ_{yy} and σ_{yz} calculated by XLWM and MSC.Nastran for the composite laminated beam with a unit pressure at the bottom surface, where the size, the load case, the boundary condition, and the discretization schemes of the composite beam with delamination are same with that employed in aforementioned numerical examples. It can be seen from Figure 11 that the maximum value and the distribution of stresses obtained by XLWM agree with the results of MSC.Nastran. The stress σ_{yz} formed severe stress concentration at the front of the delamination and nearby the boundaries.

The influence of the location in thickness direction and the size of delamination on the maximum displacements are investigated by using the XLWM. The influence of delamination location

DOI: 10.1002/nme

Table IV. Maximum displacements for the composite laminated beam with delamination in the middle of the span (CC).

		u_1 ($10^{-7}m$)		u_2 ($10^{-6}m$)	
Stacking sequences	Number of nodes	MSC	XLWM	MSC	XLWM
$[0]_8$	111	2.13887	2.15082	4.34984	4.36381
			(2.14684)		(4.38274)
	131	2.13905	2.15117	4.36242	4.36740
			(2.14814)		(4.39888)
$[0/90/0/90]_s$	111	2.97151	2.99313	6.22773	6.29975
			(2.98571)		(6.29328)
	131	2.97165	2.99440	6.24240	6.29376
			(2.98803)		(6.32132)
$[90/0/90/0]_s$	111	6.00012	6.05247	10.0818	10.2310
			(6.02489)		(10.2004)
	131	6.00068	6.05462	10.0978	10.2329
			(6.02521)		(10.2025)

XLWM, extended layerwise method.

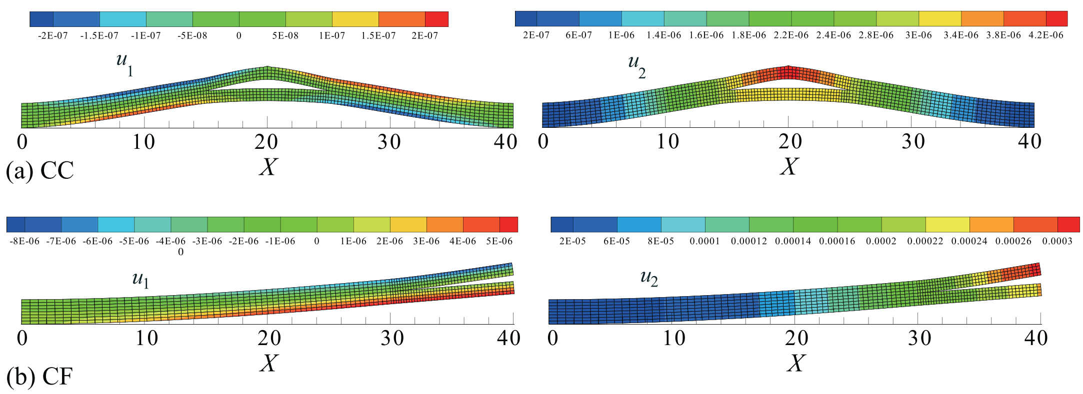

Figure 10. Deformation obtained by extended layerwise method for the composite beam $[0]_8$ with delamination. (a) one end clamp beam (CF); (b) doubly-clamp beam (CC).

along the thickness direction on the deformation and the maximum displacements are shown in Figures 12 and 13, respectively. The stacking sequence of the composite presented in Figure 13 is $[0/90/0/90]_s$. The delamination is located at the middle of the span, and vary from the first interface to the seventh interface. $u_1^{(1)}$ and $u_2^{(1)}$ are the displacements of the composite beams with delamination at the first interface. It can be seen from Figures 12 and 13 that the local deformation is more obvious as the delamination approaching to the surface of the load side. The maximum displacements of the laminated beam with stacking sequence $[90/90/90/0]_s$ are more sensitive to the location of delamination in the thickness direction than that of the other two kinds of stacking sequences $[0]_8$ and $[0/90/0/90]_s$.

For different location, the influence of delamination size on the deformation pattern and the maximum displacements are shown in Figures 14 and 15, respectively. The stacking sequence of the composite presented in Figure 14 is $[0/90/0/90]_s$. The size of the delamination is 10 mm. $u_1^{(10)}$ and $u_2^{(10)}$ are the displacements of the composite beams with delamination of 10 mm. It can be seen from Figures 12 and 13 that the local deformation is more obvious as the size of delamination is increasing. The maximum displacements increase significantly as the delamination size is increasing. As the delamination is approaching to the surface of the load side, the influence of the delamination size on the maximum displacements is more significant. When the delamination is located in the

DOI: 10.1002/nme

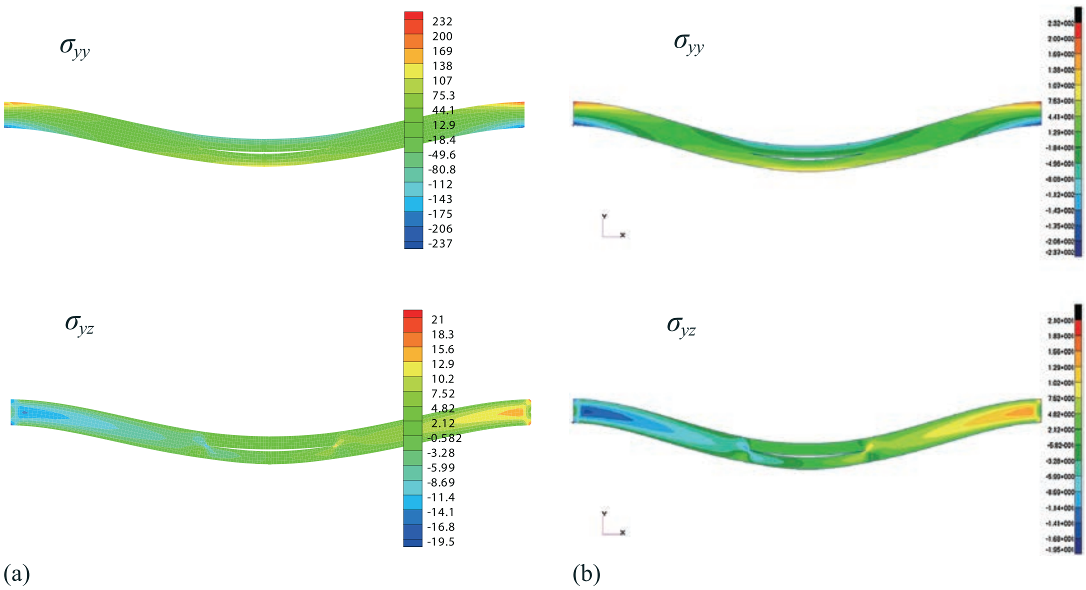

Figure 11. Stresses obtained by extended layerwise method (XLWM) and MSC for the composite beam $[0/90/0/90]_s$ with delamination. (a) XLWM; (b) MSC.

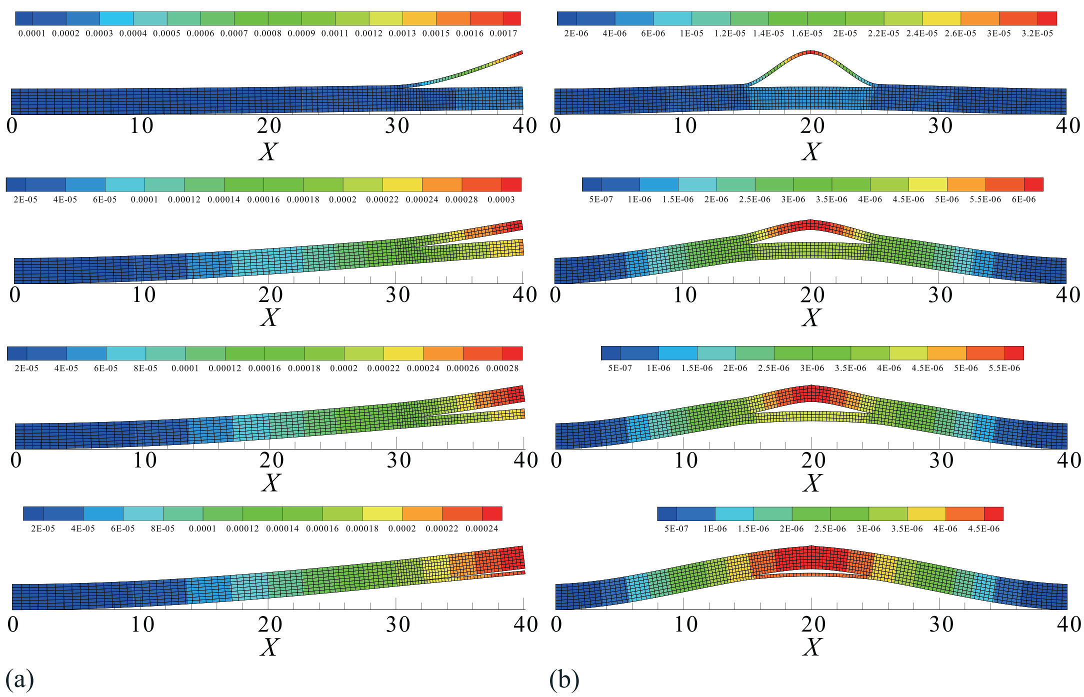

Figure 12. Influence of delamination location along the thickness direction on the deformation of composite laminated beam ($[0/90/0/90]_s$). (a)one end clamp beam (CF); (b) doubly-clamp beam (CC).

interface between second layer and third layer, the maximum displacements u_1 and u_2 of the laminated beam with stacking sequence $[90/90/90/0]_s$ and $[0/90/0/90]_s$ are more sensitive to the delamination size than that of the stacking sequences $[0]_8$. When the location of delamination in the thickness direction approaches to the reverse side of load side, the maximum displacement u_1 of the laminated beam with stacking sequence $[0]_8$ is more sensitive to the location of

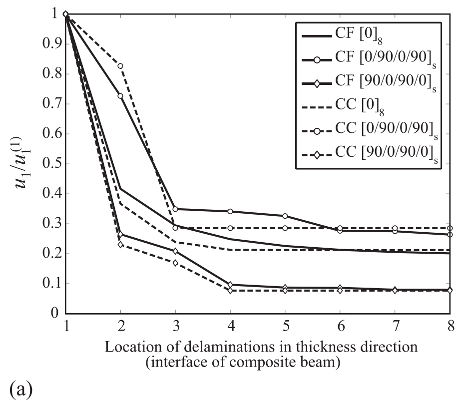

Figure 13. Influence of delamination location along the thickness direction on the maximum displacements of composite laminated beam. (a) Displacement u_1; (b) displacement u_2.

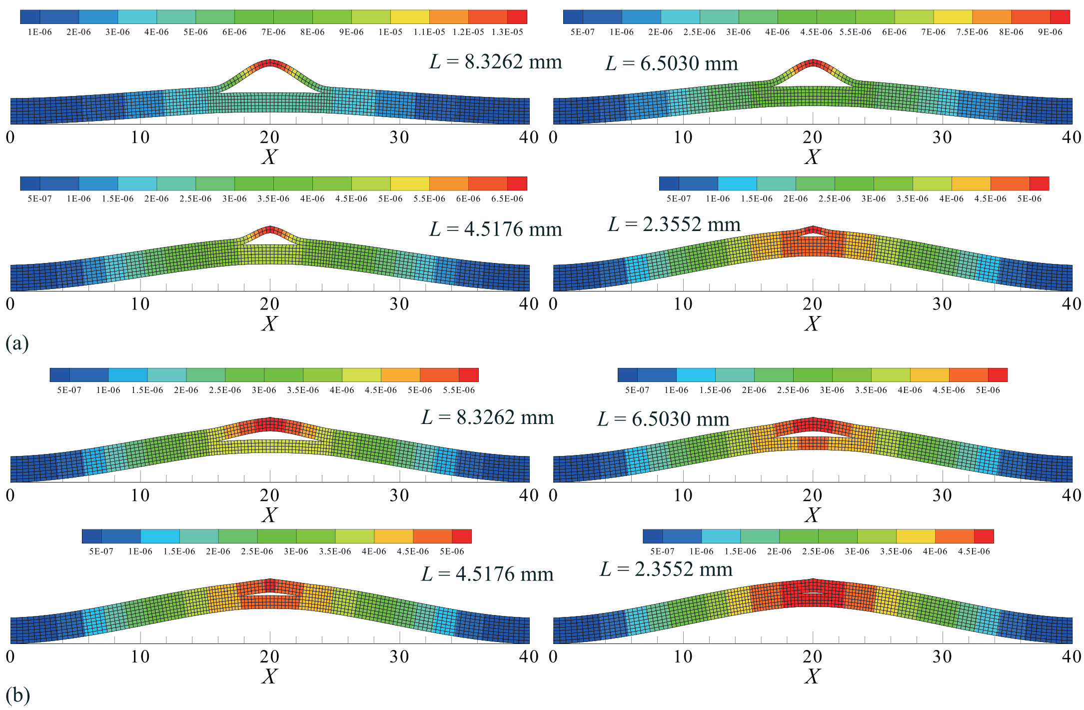

Figure 14. Influence of delamination size on the deformation of composite laminated beam with delamination. (a) The delamination is located in the interface between second and third layer; (b) The delamination is located in the interface between fourth and fifth layer.

delamination in the thickness direction than that of the other two kinds of stacking sequences $[90/90/90/0]_s$ and $[0/90/0/90]_s$. When the delamination is located in the interface between fourth layer and fifth layer, the maximum displacements of the laminated beam with stacking sequence $[0/90/0/90]_s$ are most sensitive to the delamination size. However, it is the laminated beam with stacking sequence $[90/90/90/0]_s$ when the delamination is located in the interface between sixth layer and seventh layer.

The composite laminated beams with multiple delaminations are investigated by the present method in this numerical example as well. The delaminations can be denoted as $[\theta/\theta/\cap/\theta/\theta/\cap/\theta/\theta/\cap/\theta/\theta]$ in the damage region. The stacking sequence is $[0/90/0/90]_s$. For two kinds of boundary conditions CF and CC, the deformations are plotted in Figures 16 and 17,

DOI: 10.1002/nme

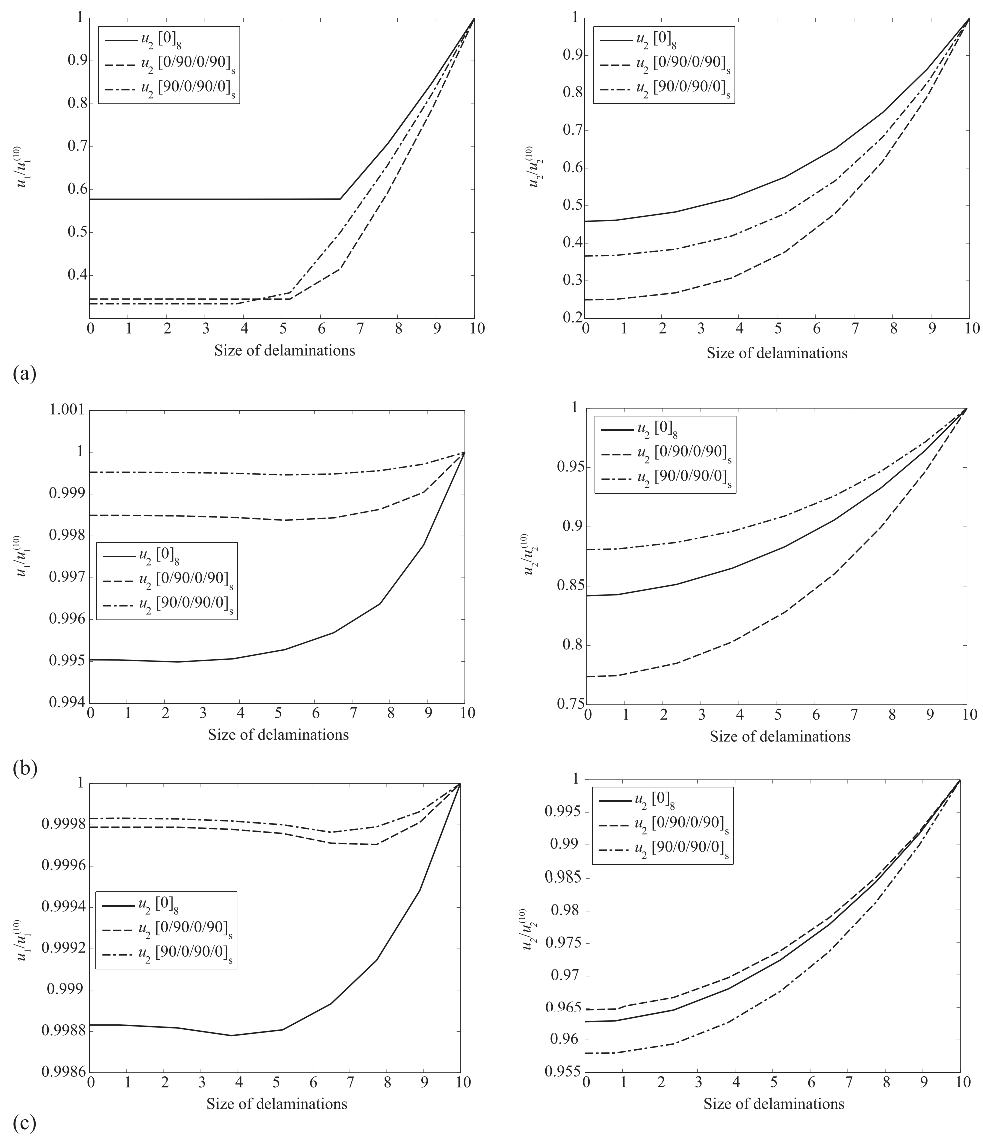

Figure 15. Influence of delamination size on the maximum displacements of composite laminated beam with delamination. (a) The delamination is located in the interface between second and third layer; (b) the delamination is located in the interface between fourth and fifth layer; and (c) the delamination is located in the interface between sixth and seventh layer.

respectively, which show that the XLWM is well suited to model the composite laminated beam with multiple delaminations.

6.3. *Composite laminated beam with in-plane matrix cracks*

In this example, a composite laminated beam with in-plane matrix cracks is investigated. Because the addition freedoms used to simulate delaminations vanish, the indices ζ and η in Equation (28) take the value of i and r, and the values of k and e depend on the value of ζ, see Equation (1).

In order to validate the present method, an isotropic beam with in-plane matrix cracks is considered. The size, the load case, and the boundary condition of the composite beam with a matrix crack in the middle of the span employed in this example are shown in Figure 18. There are two kinds of boundary conditions, CF and CC. There are four different crack depths, see the cases 1–4 in Figure 18, where $\underline{\theta}$ denotes that the tip crack is located at the middle of the single layer

DOI: 10.1002/nme

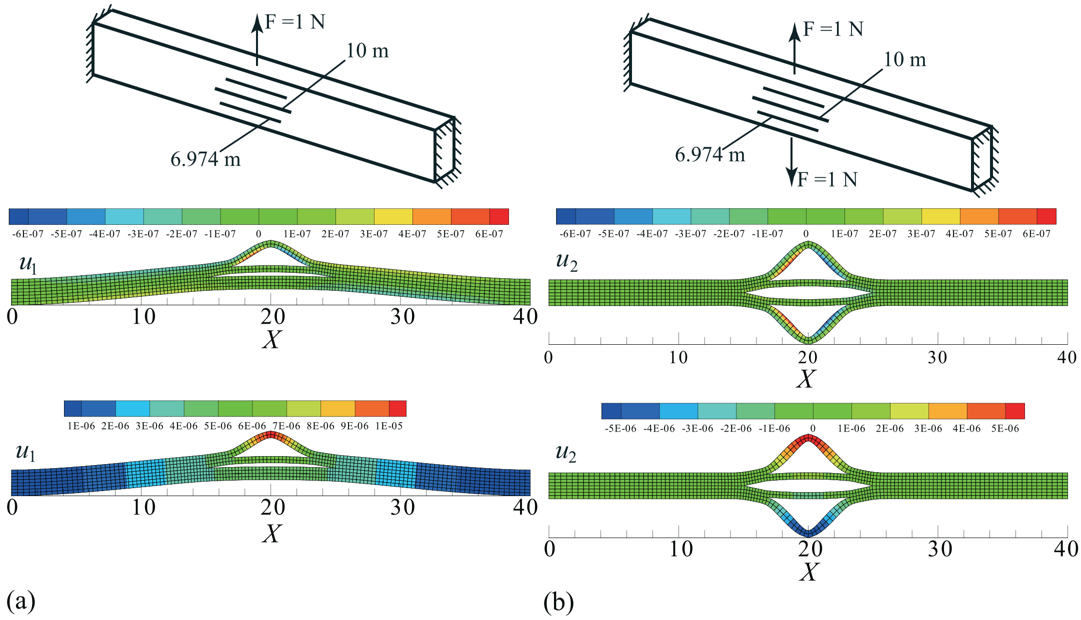

Figure 16. Deformation of composite beam ($[0/90/0/90]_s$) with multiple delaminations in the middle of the span. (a) Unsymmetrical load; (b) symmetric load.

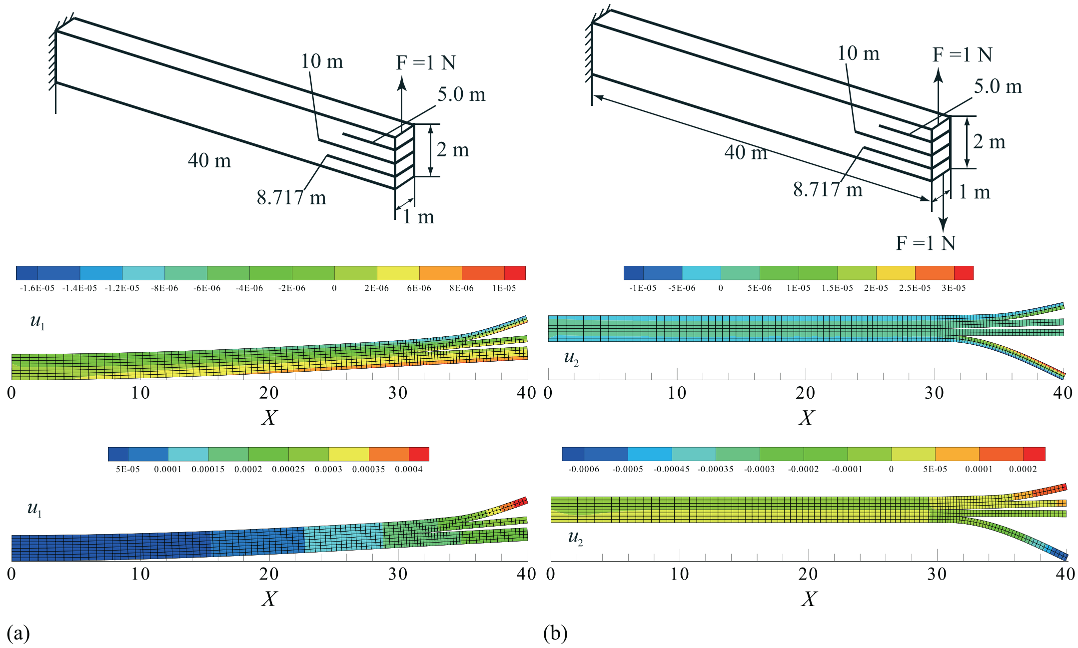

Figure 17. Deformation of composite beam ($[0/90/0/90]_s$) with multiple delaminations at the free end. (a) Unsymmetrical load; (b) symmetric load.

and bold $\boldsymbol{\theta}$ denotes that the crack cross of the single layer. The material properties are chosen as $E = 5.2 \times 10^4$MPa, $v = 0.3$.

The maximum displacements obtained by MSC.Nastran with Hex8 solid elements and the present method for the isotropic beam with in-plane matrix crack are listed in Table V. In the FEM analysis, node pairs are employed to model the in-plane matrix cracks. The isotropic beam is divided into

DOI: 10.1002/nme

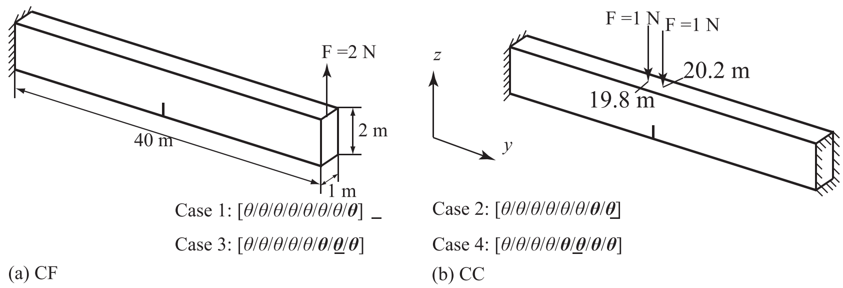

Figure 18. Composite laminated beams with in-plane matrix crack. (a) One end clamp beam (CF); (b) doubly-clamp beam (CC).

Table V. The maximum displacements for the isotropic beam with in-plane crack.

		CF				CC			
		u_1 $(10^{-5}m)$		u_2 $(10^{-3}m)$		u_1 $(10^{-6}m)$		u_2 $(10^{-5}m)$	
Case		3D elastic	XLWM	3D elastic	XLWM	3D elastic	XLWM	3D elastic	XLWM
No crack	114		4.55346		1.21266		1.42218		1.94384
	172	4.61608	4.59202	1.22959	1.22335	1.44044	1.43450	1.96762	1.96107
Case 1	114		4.63745		1.22613		1.47790		2.03352
	172	4.70263	4.67409	1.24369	1.23677	1.49919	1.49006	2.06417	2.05116
Case 2	114		4.84212		1.25429		1.59860		2.19467
	172	4.91672	4.87994	1.27307	1.26510	1.62520	1.61166	2.23275	2.21379
Case 3	114		5.25768		1.30853		1.81735		2.45192
	172	5.34736	5.29800	1.32914	1.31968	1.85066	1.83175	2.49772	2.47337
Case 4	114		6.13258		1.41652		2.18169		2.82043
	172	6.25794	6.17848	1.44134	1.42839	2.22423	2.19869	2.87611	2.84507

XLWM, extended layerwise method; CF, one end clamp beam; CC, doubly-clamp beam.

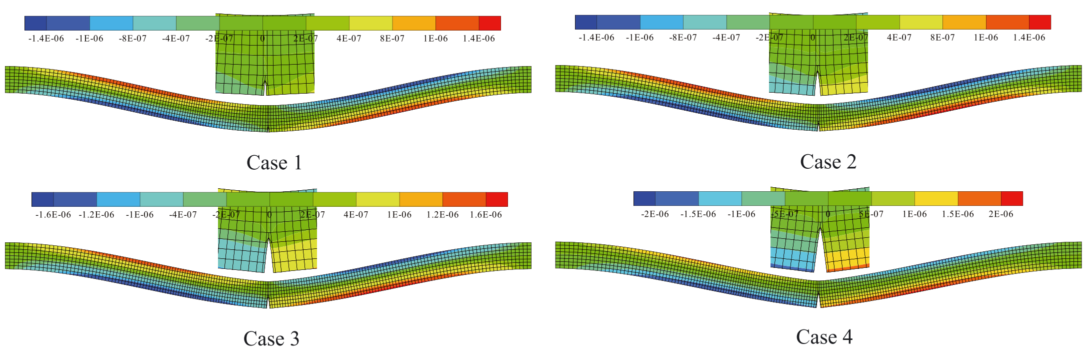

Figure 19. Deformation patterns for the isotropic beam with four different crack depth.

eight sublayers. With four different crack depths, the deformation patterns for the isotropic beam are shown in Figure 19, in which the fringes represent the distribution of displacement u_2. It is obvious that the maximum values and the fringes of the displacements obtained by present method are in good agreement with those of MSC.Nastran.

The cross-ply laminated beams with matrix cracks are studied as well. The size, the load case, and the boundary condition are shown in Figure 18. All the layers have the same thickness and material properties. The material properties of a single layer are $E_{11} = 1.81 \times 10^5$MPa, $E_{22} = E_{33} = 1.03 \times 10^4$MPa, $G_{12} = G_{13} = 7.17 \times 10^3$MPa, $G_{23} = 6.21 \times 10^3$MPa, $G_{12} = 0.28$, $G_{13} = 0.02$, $G_{23} = 0.40$. For different stacking sequences, the maximum displacements of the composite laminated beams with in-plane matrix cracks are plotted in Figure 20. The tip of the

DOI: 10.1002/nme

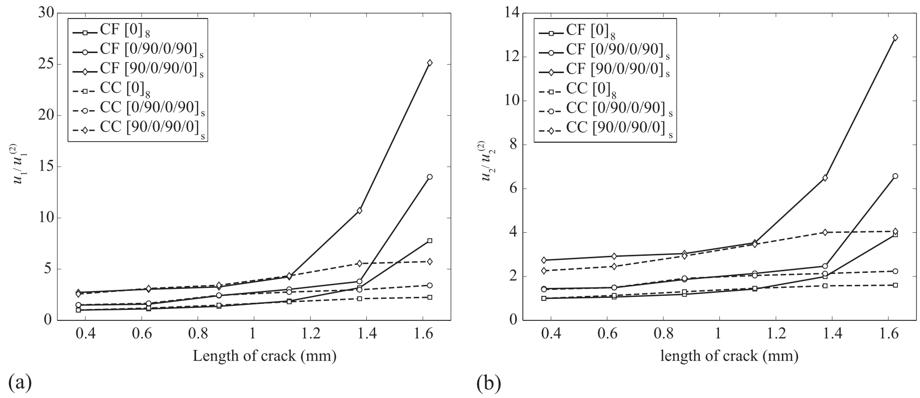

Figure 20. Effect of the crack length on the maximum displacements of the composite laminated beam with a matrix crack. (a) Displacement u_1; (b) displacement u_2.

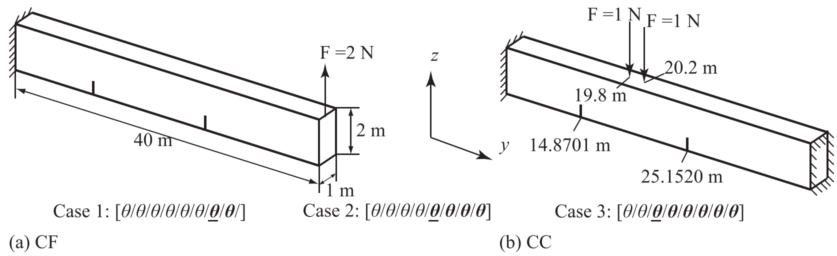

Figure 21. Composite laminated beams with multiple matrix cracks. (a) One end clamp beam (CF); (b) doubly-clamp beam (CC).

cracks changes from the middle of the second layer to the middle of the seventh layer. It can be seen from Figure 20 that the maximum displacements for both the boundary conditions CF and CC increase as the size of crack increase. The increase speed of the maximum displacements for the boundary condition CF is faster and faster as the size of crack increases, but the increase speed of the boundary condition CC is just the opposite.

The composite laminated beam with multiple matrix cracks is further investigated by the present method. The size, the load case, and the boundary condition are shown in Figure 21, where the stacking sequence is $[90/0/90/0]_s$. Three cases are studied, namely, Case 1, $[\theta/\theta/\theta/\theta/\theta/\underline{\theta}/\boldsymbol{\theta}/\boldsymbol{\theta}]$; Case 2: $[\theta/\theta/\theta/\underline{\theta}/\boldsymbol{\theta}/\boldsymbol{\theta}/\boldsymbol{\theta}/\boldsymbol{\theta}]$; and Case 3: $[\theta/\underline{\theta}/\boldsymbol{\theta}/\boldsymbol{\theta}/\boldsymbol{\theta}/\boldsymbol{\theta}/\boldsymbol{\theta}/\boldsymbol{\theta}]$. The deformation patterns of the composite beam with multiple matrix cracks are shown in Figure 22.

6.4. *Composite laminated beam with multiple delaminations and in-plane matrix cracks*

In this example, composite laminated beams with multiple in-plane matrix cracks and delaminations are investigated. In order to validate the present method, an isotropic beam with an in-plane matrix crack and a delamination in the middle of the span are considered in three cases. The size, the load case, and the boundary condition of the composite beam employed are shown in Figure 23. There are two kinds of boundary conditions, CF and CC. The material properties are taken as $E = 5.2 \times 10^4$MPa, $v = 0.3$. The isotropic beam is divided into eight layers with the same thickness. In case 1, the in-plane matrix crack and the delamination are independent, namely $[\theta/\theta/\theta/\theta/\cap/\theta/\underline{\theta}/\boldsymbol{\theta}/\boldsymbol{\theta}]$. In case 2, the in-plane matrix crack and the delamination are just intersect, namely $[\theta/\theta/\theta/\theta/\cap/\boldsymbol{\theta}/\boldsymbol{\theta}/\boldsymbol{\theta}/\boldsymbol{\theta}]$. In case 3, the in-plane matrix crack cross the delamination, namely $[\theta/\underline{\theta}/\boldsymbol{\theta}/\boldsymbol{\theta}/\cap/\boldsymbol{\theta}/\boldsymbol{\theta}/\boldsymbol{\theta}/\boldsymbol{\theta}]$.

The maximum displacements obtained by MSC.Nastran with Hex8 solid elements and the present method for the isotropic beam with in-plane matrix crack and delamination are listed in Table VI. The fringe and deformation patterns are shown in Figure 24. It can be seen from Table VI that the

DOI: 10.1002/nme

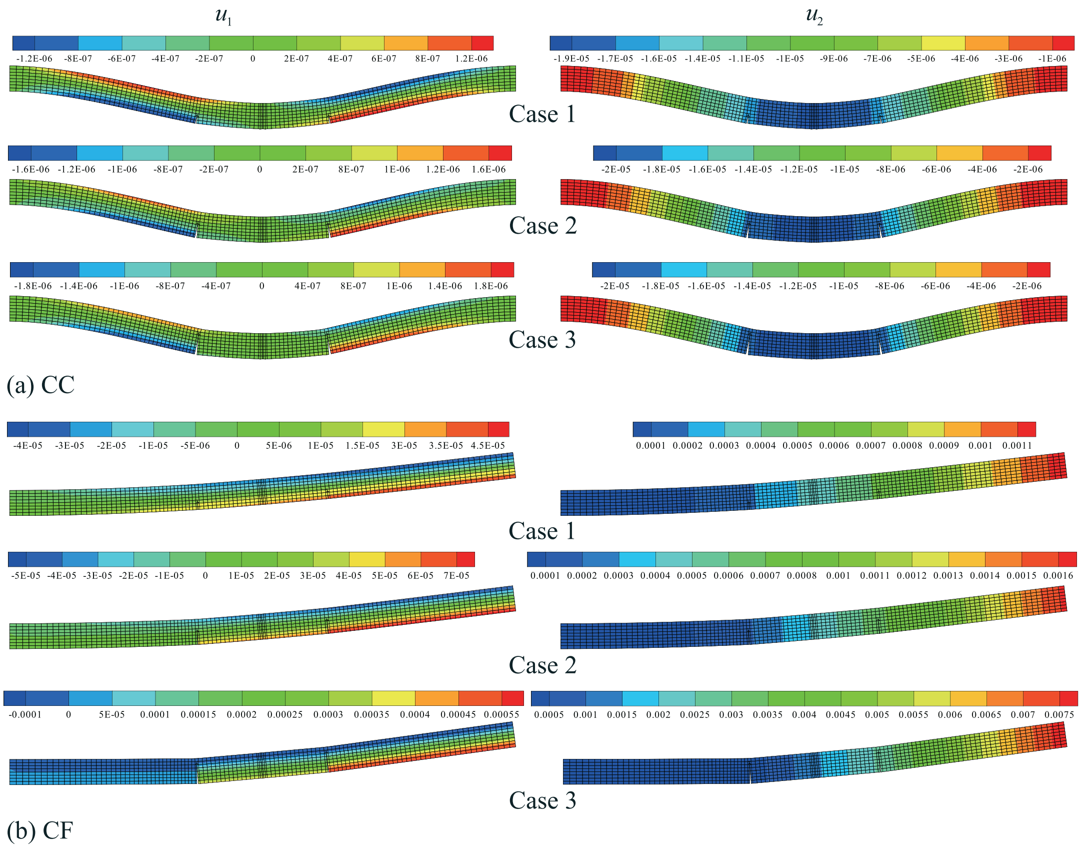

Figure 22. Deformation of composite beam $[90/0/90/0]_S$ with multiple matrix cracks. (a) One end clamp beam (CF); (b) doubly-clamp beam (CC).

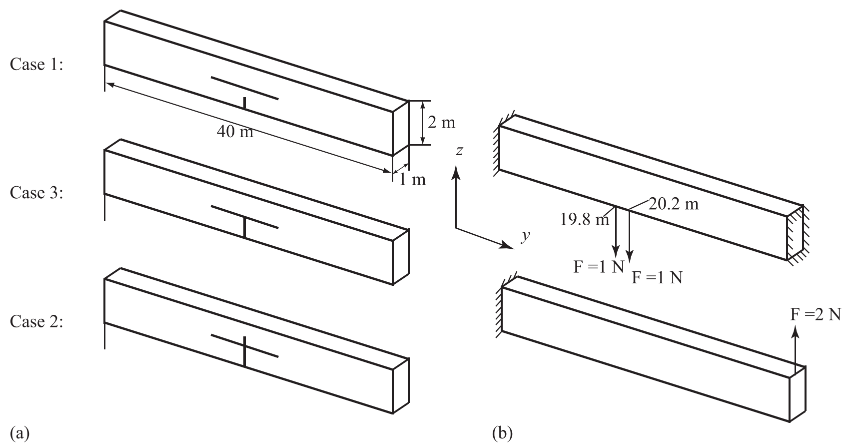

Figure 23. Composite laminated beams with in-plane matrix crack and delamination. (a) Three kinds of cases; (b) loading modes of one end clamp beam (CF) and doubly-clamp beam (CC).

increase of the maximum displacement is less than 2% as the number of the nodes increased from 79 to 101. For different boundary conditions, reasonable converged values have been achieved, but the convergence rate for boundary condition CF is faster than that for boundary condition CC. It is obvious that the maximum values and the fringes displacements obtained by present method are in good agreement with those of MSC.Nastran. The material penetration phenomenon, which is not

DOI: 10.1002/nme

Table VI. The maximum displacements obtained by FEM and XLWM for the isotropic beam with in-plane matrix crack and delamination.

		CF				CC			
		u_1 $(10^{-4}m)$		u_2 $(10^{-3}m)$		u_1 $(10^{-6}m)$		u_2 $(10^{-5}m)$	
Cases	Nodes	3D elastic	XLWM	3D elastic	XLWM	3D elastic	XLWM	3D elastic	XLWM
Case 1	114		0.52430		1.32557		2.24325		3.34366
	172	0.53613	0.52810	1.35102	1.33696	2.35240	2.26824	3.46823	3.39372
Case 2	114		1.78343		2.94517		5.38330		5.66587
	172	1.82965	1.82445	3.01921	3.00632	5.50849	5.46782	5.81501	5.78318
Case 3	114		2.6996		3.96512		5.41953		5.67657
	172	2.84072	2.7427	4.1443	4.02866	5.54002	5.49919	5.82865	5.79240

XLWM, extended layerwise method; CF, one end clamp beam; CC, doubly-clamp beam.

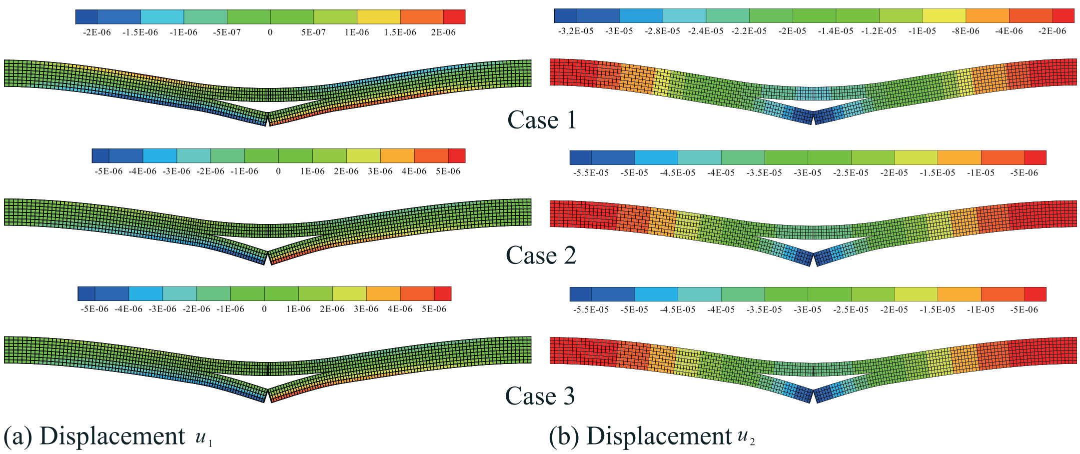

Figure 24. Fringe and deformation pattern for the composite laminated beams with in-plane matrix crack and delamination. (a) Displacement u_1 one end clamp beam (CC); (b) displacement u_2 doubly-clamp beam (CC).

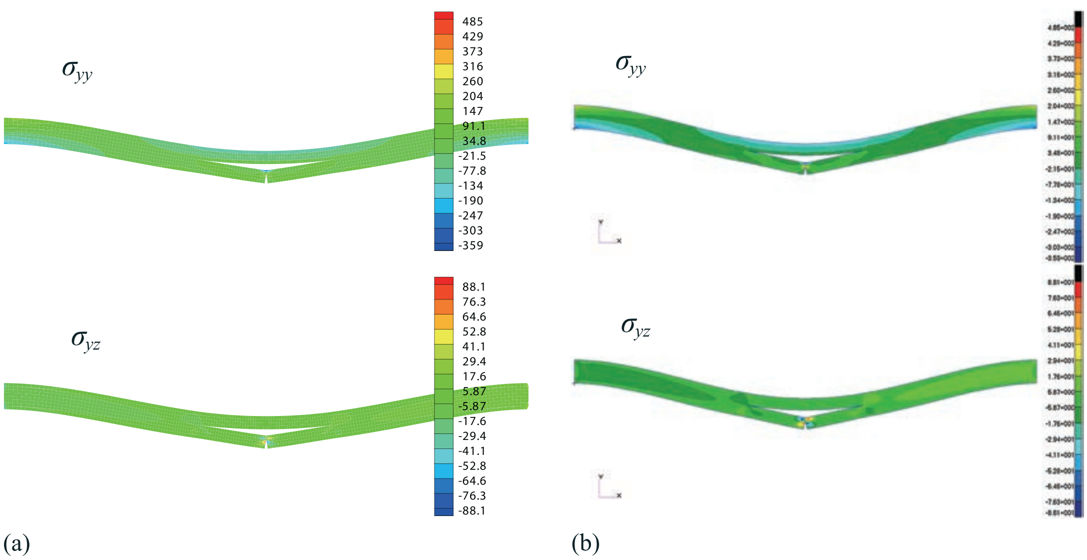

Figure 25. Stresses obtained by extended layerwise method (XLWM) and MSC for the composite laminated beams with in-plane matrix crack and delamination. (a) XLWM; (b) MSC.

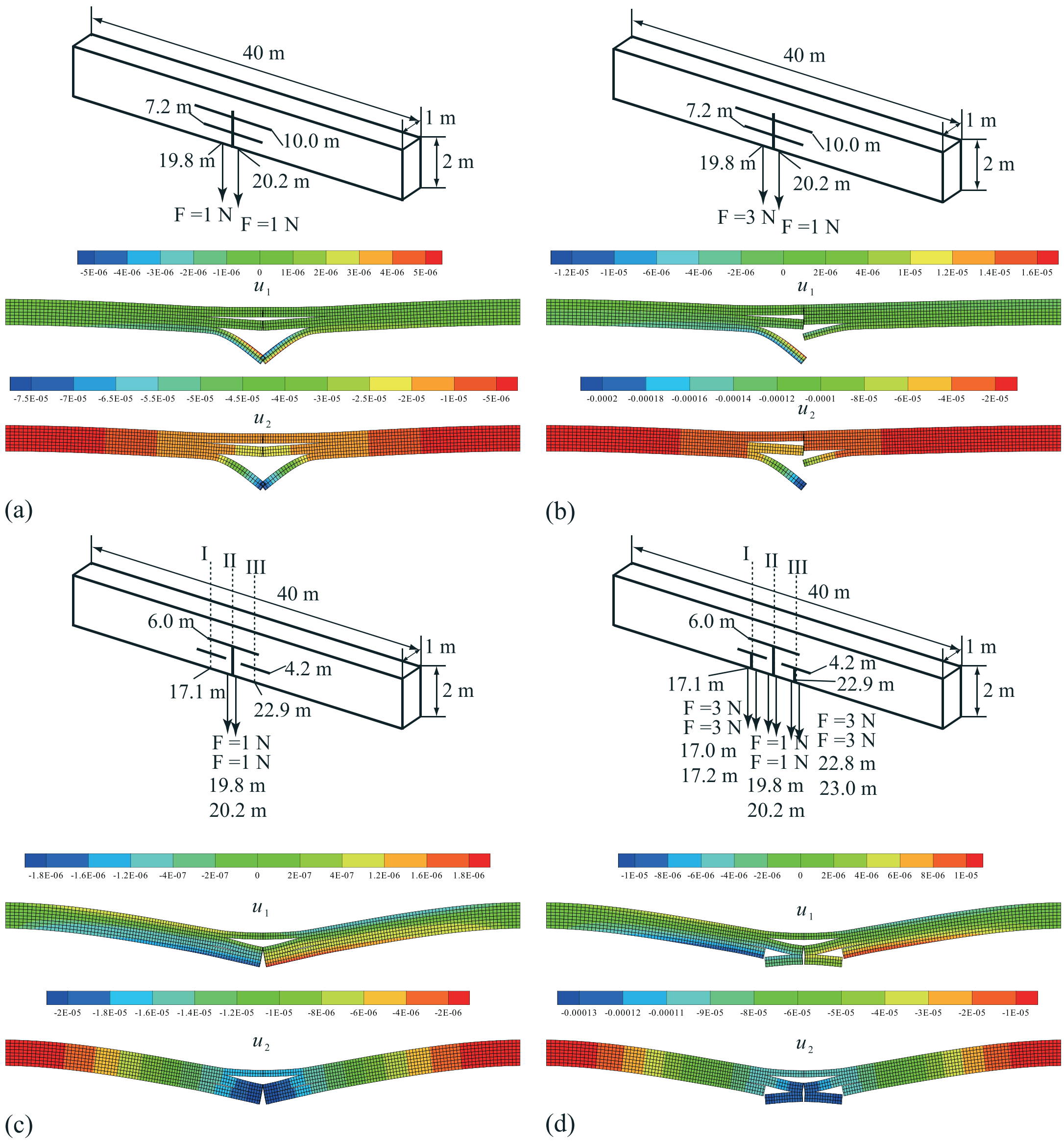

Figure 26. Fringe and deformation results calculated by the present method for the composite laminated beams $[0/90/0/90]_s$ with in-plane matrix crack and multiple delaminations.

admissible, is found in the results shown in Figure 24, because the contact behavior of the matrix crack interface has not been considered.

Figure 25 presents the comparison of the stresses σ_{yy} and σ_{yz} calculated by XLWM and MSC.Nastran for the composite laminated beam with delamination and matrix crack, where the size, the load case, the boundary condition, and the discretization schemes of the composite beam are same with that employed in aforementioned numerical example. This composite beam is subjected on a unit pressure at the bottom surface. It can be seen from Figure 25 that the maximum value and the distribution of stresses obtained by XLWM agree with the results of MSC.Nastran. The stress σ_{yz} formed severe stress concentration at the front of the delamination, nearby the boundaries and the tip of the matrix crack, while the stress σ_{yy} only formed severe stress concentration at the tip of the matrix crack.

The composite laminated beams with widespread matrix crack and multiple delaminations are studied by the XLWM to further prove its capacity to deal with the complex damage form. The

DOI: 10.1002/nme

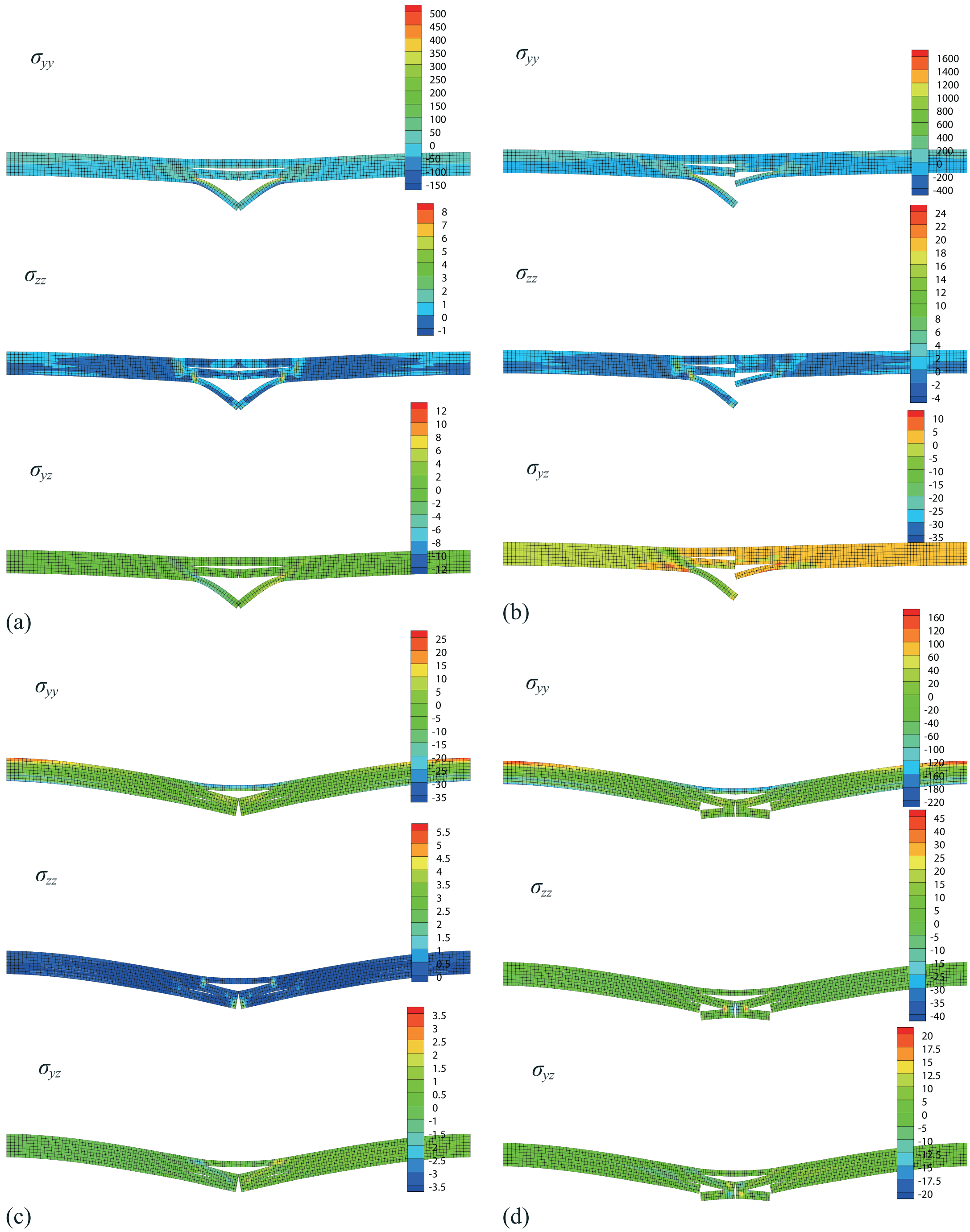

Figure 27. Stresses results calculated by the present method for the composite laminated beams $[0/90/0/90]_s$ with in-plane matrix crack and multiple delaminations.

stacking sequence is $[0/90/0/90]_s$. The material properties of the single layer are chosen as $E_{11} = 1.81 \times 10^5$MPa, $E_{22} = E_{33} = 1.03 \times 10^4$MPa, $G_{12} = G_{13} = 7.17 \times 10^3$MPa, $G_{23} = 6.21 \times 10^3$MPa, $G_{12} = 0.28$, $G_{13} = 0.02$, and $G_{23} = 0.40$. Fringe and deformation pattern are shown in Figure 26 for the composite laminated beams with the complex damage form. In Figure 26(a) and (b), the matrix crack and delamination are denoted as $[\theta/\underline{\theta}/\boldsymbol{\theta}/\cap/\boldsymbol{\theta}/\boldsymbol{\theta}/\boldsymbol{\theta}/\cap/\boldsymbol{\theta}/\boldsymbol{\theta}]$. In Figure 26(c), the matrix crack and delamination are denoted as $[\theta/\theta/\theta/\cap/\theta/\theta/\theta/\cap/\theta/\theta]$ in sections I and III, $[\theta/\underline{\theta}/\boldsymbol{\theta}/\cap/\boldsymbol{\theta}/\boldsymbol{\theta}/\cap/\boldsymbol{\theta}/\boldsymbol{\theta}/\boldsymbol{\theta}]$ in section II. In Figure 26(c), the matrix crack and delamination

DOI: 10.1002/nme

are denoted as $[\theta/\theta/\theta/\cap/\theta/\theta/\cap/\boldsymbol{\theta}/\boldsymbol{\theta}/\boldsymbol{\theta}]$ in sections I and III, $[\theta/\underline{\theta}/\boldsymbol{\theta}/\cap/\boldsymbol{\theta}/\boldsymbol{\theta}/\boldsymbol{\theta}/\cap/\boldsymbol{\theta}/\boldsymbol{\theta}]$ in section II. It can be seen from Figure 26 that the present method is capable to simulate complex damage form of the composite laminated beams. In addition, the stresses results for the composite laminated beams with multiple delaminations and widespread matrix cracks are shown in Figure 27.

7. CONCLUSION

In the present work, a new analysis method is established for the composite laminated beams with in-plane matrix cracks and multiple delaminations. Firstly, an XLWM is developed for the composite laminated beam with multiple delaminations and matrix cracks by employing a displacement field constructed with the linear Lagrange interpolation functions, the one-dimensional signed distance function and strong discontinuity function. The strong and weak discontinuity functions are applied in the displacements field along the thickness direction to model the displacement discontinuity induced by delaminations and the strain discontinuity induced by the interface between the layers, respectively.

To demonstrate the excellent predictive capability of the XLWM, several numerical examples were carried out to investigate the problem of static analysis for the composite laminated beams with multiple matrix cracks and/or delaminations. Good agreement had been achieved between the predictions and the 3D elastic results of MSC.Nastran. The results shown that the present methods are well suited to the static problem of the composite laminated structures with complex damage form. If the contact behavior of the interface of the matrix cracks and delaminations is taken into account and the virtual crack closure technique is employed to calculate the energy release rate of the delaminations front, the XLWM can be extended to predict the onset and growth of matrix cracks and delamination introduced by the low impact.

In addition, the influences of the delamination size and location on the maximum displacements are investigated for the composite laminated beams, together with the effects of the matrix crack length on the maximum displacements.

ACKNOWLEDGEMENTS

This work is supported by the National Basic Research Program of China (2010CB832701), the National Natural Science Foundation of China (11272180), and the Tsinghua University Initiative Scientific Research Program.

REFERENCES

1. Wu HYT, Chang FK. Transient dynamic analysis of laminated composite plates subjected to transverse impact. *Computers & Structures* 1989; **31**:453–466.
2. Wu HY. Impact damage of composite. *Ph.D. Thesis*, Stanford University, Stanford, California, 1986.
3. Krishnamurthy KS, Mahajan P, Mittal RK. A parametric study of the impact response and damage of laminated cylindrical composite shells. *Composites Science and Technology* 2001; **61**(12):1655–1669.
4. Gong SW, Lam KY. Transient response of stiffened composite plates subjected to low velocity impact. *Composites Part B: Engineering* 1999; **30**(5):473–484.
5. Gong SW, Toh SL, Shim VPW. The elastic response of orthotropic laminated cylindrical shells to low-velocity impact. *Composites Engineering* 1994; **4**:247–266.
6. Choi HY, Chang FK. A model for predicting damage in graphite/epoxy laminated composites resulting from low-velocity point impact. *Journal of Composite Materials* 1992; **26**(14):2134–2169.
7. Choi HY, Wu HYT, Chang FK. A new approach toward understanding damage mechanisms and mechanics of laminated composites due to low-velocity impact: part 2-analysis. *Journal of Composite Materials* 1991; **25**(8): 1012–1038.
8. Choi HY, Downs RJ, Chang FK. A new approach toward understanding damage mechanisms and mechanics of laminated composites due to low-velocity impact: part 1-experiments. *Journal of Composite Materials* 1991; **25**(8): 992–1011.
9. Abrate S. Impact on laminated composite materials. *Applied Mechanics Reviews* 1991; **44**(4):155–190.
10. Abrate S. Impact on laminated composites: recent advances. *Applied Mechanics Reviews* 1994; **47**(11):517–544.
11. Richardson MOW, Wisheart MJ. Review of low-velocity impact properties of composite materials. *Composites Part A: Applied Science and Manufacturing* 1996; **27**(12):1123–1131.

DOI: 10.1002/nme

12. Joshi SP, Sun CT. Impact induced fracture in a laminated composite. *Journal of Composite Materials* 1985; **19**(1): 51–66.
13. Highsmith AL, Reifsnider KL. Stiffness-reduction mechanisms in composite laminates. *Damage in Composite Materials, ASTM STP* 1982; **775**:103–117.
14. Laws N, Dvorak GJ, Hejazi M. Stiffness changes in unidirectional composites caused by crack systems. *Mechanics of Materials* 1983; **2**(2):123–137.
15. Laws N, Dvorak GJ. Progressive transverse cracking in composite laminates. *Journal of Composite Materials* 1988; **22**(10):900–916.
16. Wang ASD, Chou PC, Lei SC. A stochastic model for the growth of matrix cracks in composite laminates. *Journal of Composite Materials* 1984; **18**(3):239–254.
17. Hashin Z. Analysis of cracked laminates: a variational approach. *Mechanics of Materials* 1985; **4**(2):121–136.
18. Hashin Z. Analysis of orthogonally cracked laminates under tension. *Journal of Applied Mechanics* 1987; **54**(4): 872–879.
19. Aboudi J. Stiffness reduction of cracked solids. *Engineering Fracture Mechanics* 1987; **26**(5):637–650.
20. Lee JW, Allen DH, Harris CE. Internal state variable approach for predicting stiffness reductions in fibrous laminated composites with matrix cracks. *Journal of Composite Materials* 1989; **23**(12):1273–1291.
21. Gudmundson P, Weilin Z. An analytic model for thermoelastic properties of composite laminates containing transverse matrix cracks. *International Journal of Solids and Structures* 1993; **30**(23):3211–3231.
22. Hashin Z. Failure criteria for unidirectional fiber composites. *Journal of Applied Mechanics* 1980; **47**(2):329–334.
23. Hashin Z. Analysis of composite materials-A Survey. *Journal of Applied Mechanics* 1983; **50**(3):481–505.
24. Barbero EJ, Reddy JN. Modeling of delamination in composite laminates using a layer-wise plate theory. *International Journal of Solids and Structures* 1991; **28**(3):373–388.
25. Chattopadhyay A, Gu H. New higher order plate theory in modeling delamination buckling of composite laminates. *AIAA Journal* 1994; **32**(8):1709–1716.
26. Williams TO. A generalized multilength scale nonlinear composite plate theory with delamination. *International Journal of Solids and Structures* 1999; **36**(20):3015–3050.
27. Williams TO, Addessio FL. A general theory for laminated plates with delaminations. *International Journal of Solids and Structures* 1997; **34**(16):2003–2024.
28. Cho M, Kim JS. Higher-order zig-zag theory for laminated composites with multiple delaminations. *Journal of Applied Mechanics* 2001; **68**(6):869–877.
29. Kim JS, Cho M. Buckling analysis for delaminated composites using plate bending elements based on higher-order zig-zag theory. *International Journal for Numerical Methods in Engineering* 2002; **55**(11):1323–1343.
30. Azdoud Y, Han F, Lubineau G. A morphing framework to couple non-local and local anisotropic continua. *International Journal of Solids and Structures* 2013; **50**(9):1332–1341.
31. Lubineau G, Azdoud Y, Han F, Rey C, Askari A. A morphing strategy to couple non-local to local continuum mechanics. *Journal of the Mechanics and Physics of Solids* 2012; **60**(6):1088–1102.
32. O'Brien TK. Analysis of local delaminations and their influence on composite laminate behavior. *Delamination and Debonding of Materials, ASTM STP* 1985; **876**:282–297.
33. Dharani LR, Tang H. Micromechanics characterization of sublaminate damage. *International Journal of Fracture* 1990; **46**(2):123–140.
34. Nairn JA, Hu S. The initiation and growth of delaminations induced by matrix microcracks in laminated composites. *International Journal of Fracture* 1992; **57**(1):1–24.
35. Takeda N, Ogihara S. Initiation and growth of delamination from the tips of transverse cracks in cfrp cross-ply laminates. *Composites Science and Technology* 1994; **52**(3):309–318.
36. Berthelot JM, Le Corre JF. A model for transverse cracking and delamination in cross-ply laminates. *Composites Science and Technology* 2000; **60**(7):1055–1066.
37. Ladevze P, Lubineau G. pont entre les micro et méso mécaniques des composites stratifiés. *Comptes Rendus Mcanique* 2003; **331**(8):537–544.
38. Ladevze P, Lubineau G, Marsal D. Towards a bridge between the micro- and mesomechanics of delamination for laminated composites. *Composites Science and Technology* 2006; **66**(6):698–712.
39. Swindeman MJ. A regularized extended finite element method for modeling the coupled cracking and delamination of composite materials. *Ph.D. Thesis*, University of Dayton, Dayton, Ohio, 2011.
40. Belytschko T, Black T. Elastic crack growth in finite elements with minimal remeshing. *International Journal for Numerical Methods in Engineering* 1999; **45**(5):601–620.
41. Dolbow J, Belytschko T. A finite element method for crack growth without remeshing. *International Journal for Numerical Methods in Engineering* 1999; **46**(1):131–150.
42. Dolbow J, Moës N, Belytschko T. An extended finite element method for modeling crack growth with frictional contact. *Computer Methods in Applied Mechanics and Engineering* 2001; **190**(51):6825–6846.
43. Moës N, Gravouil A, Belytschko T. Non-planar 3d crack growth by the extended finite element and level sets part I: mechanical model. *International Journal for Numerical Methods in Engineering* 2002; **53**(11):2549–2568.
44. Sukumar N, Chopp DL, Moran B. Extended finite element method and fast marching method for three-dimensional fatigue crack propagation. *Engineering Fracture Mechanics* 2003; **70**(1):29–48.
45. Duan Q, Song JH, Menouillard T, Belytschko T. Element-local level set method for three-dimensional dynamic crack growth. *International Journal for Numerical Methods in Engineering* 2009; **80**(12):1520–1543.

DOI: 10.1002/nme

46. Areias P, Belytschko T. Non-linear analysis of shells with arbitrary evolving cracks using xfem. *International Journal for Numerical Methods in Engineering* 2005; **62**(3):384–415.
47. Dolbow J, Moës N, Belytschko T. Modeling fracture in Mindlin–Reissner plates with the extended finite element method. *International Journal of Solids and Structures* 2000; **37**(48):7161–7183.
48. Zhuang Z, Cheng BB. Development of x-fem methodology and study on mixed-mode crack propagation. *Acta Mechanica Sinica* 2011; **27**(3):406–415.
49. Zhuang Z, Cheng BB. A novel enriched cb shell element method for simulating arbitrary crack growth in pipes. *Science China Physics, Mechanics and Astronomy* 2011; **54**(8):1520–1531.
50. Sukumar N, Huang ZY, Prévost JH, Suo Z. Partition of unity enrichment for bimaterial interface cracks. *International Journal for Numerical Methods in Engineering* 2004; **59**(8):1075–1102.
51. Hettich T, Ramm E. Interface material failure modeled by the extended finite-element method and level sets. *Computer Methods in Applied Mechanics and Engineering* 2006; **195**(37):4753–4767.
52. Esna Ashari S, Mohammadi S. Modeling delamination in composite laminates using xfem by new orthotropic enrichment functions. *IOP Conference Series: Materials Science and Engineering,* Sidney, Australia 2010; **10**(1):012240.
53. Esna Ashari S, Mohammadi S. Fracture analysis of frp-reinforced beams by orthotropic xfem. *Journal of Composite Materials* 2012; **46**(11):1367–1389.
54. Asadpoure A, Mohammadi S, Vafai A. Crack analysis in orthotropic media using the extended finite element method. *Thin-Walled Structures* 2006; **44**(9):1031–1038.
55. Asadpoure A, Mohammadi S, Vafai A. Modeling crack in orthotropic media using a coupled finite element and partition of unity methods. *Finite Elements in Analysis and Design* 2006; **42**(13):1165–1175.
56. Asadpoure A, Mohammadi S. Developing new enrichment functions for crack simulation in orthotropic media by the extended finite element method. *International Journal for Numerical Methods in Engineering* 2007; **69**(10): 2150–2172.
57. Motamedi D, Mohammadi S. Dynamic crack propagation analysis of orthotropic media by the extended finite element method. *International Journal of Fracture* 2010; **161**(1):21–39.
58. Motamedi D, Mohammadi S. Dynamic analysis of fixed cracks in composites by the extended finite element method. *Engineering Fracture Mechanics* 2010; **77**(17):3373–3393.
59. Motamedi D, Mohammadi S. Fracture analysis of composites by time independent moving-crack orthotropic {XFEM}. *International Journal of Mechanical Sciences* 2012; **54**(1):20–37.
60. Bayesteh H, Mohammadi S. {XFEM} fracture analysis of orthotropic functionally graded materials. *Composites Part B: Engineering* 2013; **44**(1):8–25.
61. Hosseini SS, Bayesteh H, Mohammadi S. Thermo-mechanical {XFEM} crack propagation analysis of functionally graded materials. *Materials Science and Engineering: A* 2013; **561**(0):285–302.
62. Esna Ashari S, Mohammadi S. Delamination analysis of composites by new orthotropic bimaterial extended finite element method. *International Journal for Numerical Methods in Engineering* 2011; **86**(13):1507–1543.
63. Nagashima T, Suemasu H. X-fem analyses of a thin-walled composite shell structure with a delamination. *Computers & Structures* 2010; **88**(9):549–557.
64. Curiel Sosa JL, Karapurath N. Delamination modelling of glare using the extended finite element method. *Composites Science and Technology* 2012; **72**(7):788–791.
65. Reddy JN. *Mechanics of Laminated Composite Plates and Shells: Theory and Analysis*. CRC Press: New York, Washington, D. C., 2003.
66. Barbero EJ, Reddyt JN. General two-dimensional theory of laminated cylindrical shells. *AIAA J* 1990; **28**(3): 544–553.
67. Owen DRJ, Li ZH. A refined analysis of laminated plates by finite element displacement methods II. Fundamentals and static analysis. *Computers & Structures* 1987; **26**(6):907–914.
68. Owen D, Li ZH. A refined analysis of laminated plates by finite element displacement methods ii. Vibration and stability. *Computers & Structures* 1987; **26**(6):915–923.
69. Epstein M, Glockner PG. Nonlinear analysis of multilayered shells. *International Journal of Solids and Structures* 1977; **13**(11):1081–1089.
70. Epstein M, Huttelmaier HP. A finite element formulation for multilayered and thick plates. *Computers & Structures* 1983; **16**(5):645–650.
71. Kassegne SK, Reddy JN. A layerwise shell stiffener and stand-alone curved beam element. *Asian Journal of Structural Engineering* 1997; **2**(1):1–14.

DOI: 10.1002/nme